In vivo biodistribution of fluorescent nanocolloids intended for drug delivery.

Evaluation of PEGylation state and fluorophore incorporation approach.

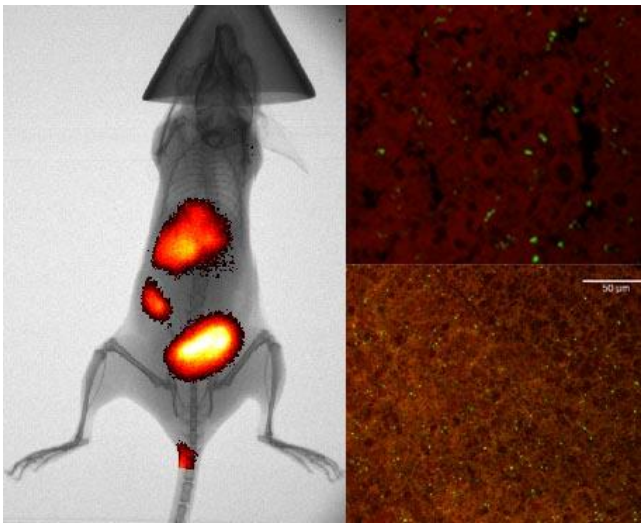

Silje Storås Milankovic.

A thesis submitted in partial fulfilment of the requirements for the degree of Master of Pharmacy

Centre for Pharmacy

Department of Biomedicine

University of Bergen

31.05.2012

Front illustration:

Left: NIR image overlaid on x-ray image of mouse injected with solid nanoparticles conjugated with DY-700

Upper right: Confocal image of liver from mouse injected with solid nanoparticles conjugated to rhodamine

Lower right: Confocal image of brown adipose tissue from mouse injected with solid nanoparticles conjugated to rhodamine

Acknowledgments

This thesis is written as a partial fulfilment of the requirements for my degree in pharmacy. The practical part was conducted from August 2011 to May 2012 at the Institute for Biomedicine with support from the Faculty of Medicine and Dentistry and the Centre for Pharmacy, University of Bergen.

First, I would like to thank my supervisors, Stein Ove Døskeland, Lars Herfindal and Emmet McCormack for sharing their knowledge, and introducing me to such a fascinating area of research. Your encouragement and many stimulating discussions are highly appreciated. I would like to thank Lars Herfindal especially for all his help and good advice, for always being available for questions and for excellent guidance during the writing of this thesis.

Many thanks go to Lene Vikebø for teaching me how to shave the animals, and a lot of technical support during the imaging. You are outstanding! I would also like to thank all the other lab personnel at the TSG lab for a fun and supportive work environment. I will miss you all.

I would like to thank my fellow master students at the institute of Biomedicine for support, understanding and good conversations during the year. I also have to thank all my fellow pharmacy students, many close friends, for encouragement, support and for five great years together.

Finally, a lot of gratitude goes to my husband Dragan Milankovic and our daughter Rebekka for vital support, and for always believing in me. I also have to tank my father, Oskar Storås, for driving me up to the mice at night on many occasions.

I could never have done this without any you!

Silje Storås Milankovic

Bergen, May 2012

Abbreviations:

BBB	Blood brain barrier
DAPI	4',6-diamidino-2-phenylindole DNA fluorescent stain
DLS	Dynamic light scatterer
DNA	Deoxyribonucleic acid
EPR	Enhanced permeability and retention (effect)
FDA	Food and Drugs Administration
FUS	Focused ultrasound surgery
GH	General healthcare
i.v.	Intravenously
ICG	indocyanine green
IR	Infrared
Mn	number average molecular weight
MPS	Mononuclear phagocyte system
MRI	Magnetic resonance imaging
mV	Milli-volts
Mw	Molecular weight
NIR	Near Infrared
Nm	Nanometers
PDI	Polydispersity index.
PEG	polyethylene glycol
PEO	polyethylene oxide
PGA	Poly (glycolic acid)
PLA	Poly (lactic acid)
PLGA	poly (lactic-co-glycolic acid)
PVA	Poly vinyl alcohol
QD's	Quantum dots
RES	Reticuloendothelial system
RPM	Revolutions per minute
SDS	Sodium dodecyl sulfate
SEM	Standard deviation of the mean
TTA	Tetradecylthioacetic acid
UV	Ultra violet (light)
VEGF	vascular endothelial growth factor,
Z average (size)	Also known as the cumulants means. Intensity averaged particle diameter.

Abstract

To move the use of PLGA nanocolloids from laboratories towards the use in humans require careful investigations around pharmacokinetics and biodistributions. The biodistributions of the nanocolloids can be traced through NIR *in vivo* imaging in a non-invasive manner. In the present study the biodistributions of two types of PLGA nanocolloids were compared, nanocapsules with an oily core loaded with carbocyanine dyes and solid nanoparticles with the fluorescent dye covalently linked. The nanocolloids were produced by nanoprecipitation; all were of injectable sizes, showed monodispersity and negative zeta potentials.

The biodistributions of DiD dye loaded nanocapsules with an oily core and solid nanoparticles conjugated to the dye DY-700 were injected in mice, and followed over 24 hours through NIR imaging, before organs were collected and imaged. Bone marrow was also collected. Solid nanoparticles were also made with a polymer covalently linked to rhodamine. After 24 hours the organs were collected for further *ex vivo* analysis by confocal microscopy.

The nanocolloids seemed to accumulate mainly in the liver, spleen and the intestine. The accumulation developed differently, and the PEGylated nanocarriers showed indications of longer circulation times, and lower accumulation in the liver. The oily core nanocapsules showed fluorescence accumulation in the bones, which was not seen with the solid nanocapsules. This was confirmed by quantification of fluorescence in collected bone marrow. This, together with accumulation in the intestine and fluorescence lifetime investigations suggested that DiD loaded nanocapsules release some dye. In line with this nanocolloids with the fluorescent dye covalently linked did not accumulate in the bone marrow, and to a small degree in the intestine. The *ex vivo* investigations were in concurrence with the results seen *in vivo.* PEGylated nanoparticles dominated in the spleen and brown adipose tissue whereas unPEGylated nanoparticles dominated in the liver and lungs.

Taken together, this study give insight in the biodistributions of nanocolloids intended for incorporation of chemotherapeutics, and also one has to be careful when choosing fluorescence labelling approach for *in vivo* detection of nanoparticles.

Contents:

1. Introduction

1.1 Introduction to nanocolloids:

Polymeric nanocolloids are promising drug delivery systems for drugs with low aqueous solubility or detrimental side effects. They can be used as slow release carriers or they can have ligands for site-specific delivery. Nanocolloids could increase solubility, decrease degradation during circulation and concentrate the drug at the desired site of action, while decreasing unwanted side effects, and all these features can be incorporated in one nanocolloid [1]. Both small molecular weight drugs and larger biological macromolecules such as DNA and proteins can be incorporated into nanocolloids. Together with targeted delivery, nanocolloids can incorporate a trigger, such as pH sensitivity, that leads to release of the active agent only when the desired site of action is reached [2].

Nanocolloids are particles in the colloidal size range, normally recognized as between 1 and 1000 nm. Drugs can be encapsulated, adsorbed, dispersed in or chemically bound to the polymer [3]. Some believe that the active agents should be encapsulated inside or bound to the colloid. Adsorption of the active agent to the particles after formation is often effective *in vitro*, but fails *in vivo* due to interactions with the reticuloendothelial system (RES). Macrophages quickly remove the active agents from the surface of the particles [1].

Nanocolloids can consist of materials such as lipids, polymers and inorganic materials and numerous nanocolloid assemblies have been developed [4]. Nanocolloids should be made of non toxic materials that have a safe route of degradation. This is not always the case, for example are quantum dots (QD's) made from inorganic materials such as cadmium selenide and zinc sulphide [5]. QD's are very stable in the body and have been shown to exhibit cytotoxicity including apoptosis [6]. QD's could cause accumulation in the body, with unknown effects at this stage. Moreover, the nanocolloids are too large to be excreted by glomeluar filtration, something which promotes longer circulation times, but also requires an alternative route of excretion [1].

The small sizes of the nanocolloids allow them to be injected intravenously, as they will not block the veins [3]. The small size is promising also for the development of pulmonary and trans-dermal drug delivery systems. It has been found that colloids under 200 nm in diameter

show a decreased rate of clearance and an increased circulation time. This is believed to be due to the large radius of curvature of the colloid that prevents binding of opsonins [3]. Examples of systems produced are liposomes, micelles, solid nanoparticles (Figure 1.1A), nanocapsules (Figure 1.1 B), solid lipid nanoparticles, microemulsions and carbon nanotubes. Liposomes are also promising as drug carriers, but are prone to rapid leakage of water-soluble drugs, and their stability and ability to control release is lower than for polymeric nanoparticles [4].

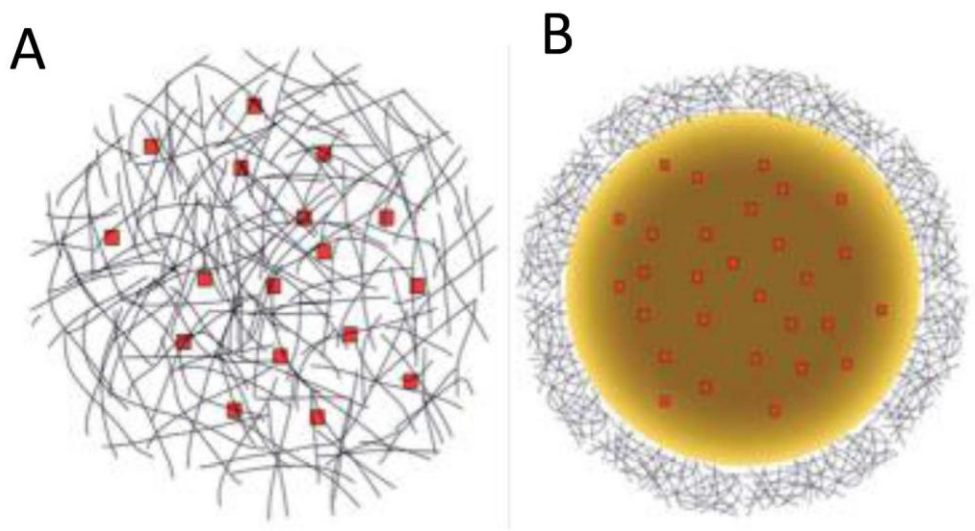

Figure 1.1 *Panel A shows the structure of solid nanoparticles (nanospheres). The drug is captured in or adsorbed on to the polymer matrix. Panel B shows the structure of a nanocapsule, where a layer of polymer surrounds an oily core that holds a lipophillic drug. Taken from [7]*

The nanocolloid should exhibit stability under physiological conditions. The nanoparticles and its surface functionalisations must have the ability to resist and traverse the physiological environment [1]. The nanocolloids often have hydrophilic molecules such as polyethylene glycol (PEG) adsorbed or bound to the surface but other surface coatings such as albumin and chitosan have also been tried [8]. The surface coatings aid in the steric stabilisation of the colloids and in addition they are meant to prevent adhesion of opsonins, and render the nanocolloids "stealth" from the macrophages in the blood. PEG chains create a highly water bound barrier which blocks the adhesion of opsonins [3].This further promotes long circulation times.

Several drug formulations using polymeric nanocolloids are already used in the clinical, such as Abraxane, where the chemotherapeutic paclitaxel is bound to albumin, which is formulated

into nanocapsules [9]. Abraxane is indicated as a secondary treatment for metastatic breast cancer where standard treatment has failed [10]. Abraxane is an example of a nanocolloid produced with a natural occurring species. Other natural occurring polymers such as the complex sugars (hyaluronan and chitosan) and inorganics (hydroxyapatite) has also been used to produce nanocolloids [11]. In this study a synthetic biodegradable polymer, poly (lactic-co-glycolic acid) (PLGA) that belongs to the α-hydroxy acids polymer family was used. Another synthetic polymer in use is the polyanhydrides [11], the early described nanoparticles were mainly formulated from poly (alkylcyanoacrylate) [4].

In this thesis it has been focused on the use of nanocolloids that can be used as drug carriers for chemotherapeutics that have low aqueous solubility and/or toxic side effects. The use of nanocolloids as drug carriers for chemotherapeutics and as a research and diagnostic tool for tumours have received much attention due to the enhance permeability and retention (EPR) effect. Solid tumour tissue has enhanced vasculature permeability due to release of vascular endothelial growth factor, VEGF, and exhibit extravasation of macromolecules, including plasma proteins and liposomes. Clearance from the interstitial space of the tumour is slow, and the macromolecules are retained for a prolonged time [12]. This is also known as passive targeting.

Nanocolloids are also promising as a tool in drug development and as diagnostic or research tool used as optical imaging contrast agents. Optical imaging includes methods such as magnetic resonance imaging (MRI), ultrasound and fluorescent optical imaging. ^{1}H-MRI is useful for detecting tumours and measuring morphological parameters. The sensitivity is low, but spatial resolution is good, and multiple sessions are possible. Super paramagnetic iron oxide nanoparticles, an MIR contrast agent, have been encapsulated together with the near infrared dye indocyanine green (ICG) into multimodal PLGA nanoparticles for use with MRI and fluorescent optical imaging [13]. But the method is costly, and only available at specialized animal facilities [14]. MRI is commonly used in hospitals, and contrast agents developed could be moved to the clinics more easily than NIR fluorescent imaging contras agents, which is more rarely used in humans. Nanocolloids could also be used to further develop and enhance techniques such as high-intensity focused ultrasound ablation, also known as focused ultrasound surgery (FUS) [15]. PLGA nanoparticles with super paramagnetic iron oxide that allow real time image guidance during FUS and to give the high resolution images obtainable with MRI have been developed [15].

The use of nanocolloids in *in vivo* fluorescence imaging has been particularly explored, and is utilised in this study. When the nanocolloids are associated with NIR contrast agents their movement *in vivo* can be traced through NIR optical imaging. There is low autofluorescence from the main tissue adsorbing components and water in the NIR window (700-1100 nm), and NIR light penetrates deeper into and out from tissues than does UV, visible or far IR light [6]. NIR contrast agents can be used with or without drugs in the nanocolloids, and the movement and accumulation in tissues such as tumours can be traced through a minimally invasive, nonionising method [6]. When both therapeutic agent and an imaging probe are combined in a nanocolloid, they are often termed multimodal or multifunctional nanocolloids [16]. Such multimodal nanocolloids could be envisioned to contain an fluorescent dye, a specific targeting agent, one or more drugs, a cell penetrating agent, a stimulus sensitive agent or any combination of these [17]. When both a diagnostic tool and a therapeutic are combined in this way it is called theranostics.

To be useful as drug delivery systems, the pharmaceutical industry needs nanocolloids that exhibit biocompatibility, biodegradation, encapsulation of the active therapeutic, colloidal stability, improved pharmacokinetics and controlled-release kinetics. None of the nanocolloids made to date fulfils all of these demands [1]. The successful transition of nanocolloids as contrast agents from the laboratories to use in the clinics requires more information around the biodistributions, clearance and biocompatibility of the nanocolloids [16].

1.2 Biodegradable nanocolloids made from PLGA

Some of the most widely used polymers used for nanocolloid are the linear, aliphatic polyesters such as PLGA, which is the co-polymer of PLA (poly lactic acid) and PGA (poly glycolic acid) (Figure 1.2). PLGA is well characterized, has long clinical experience and is commercially used for microparticulate and nanocolloid drug delivery systems. PLGA is biocompatible, biodegradable and is approved by the FDA for use in humans. In the body it undergoes hydrolysis to lactic and glycolic acid (Figure 1.2), species that are known to the organism, and are further eliminated by the normal metabolic pathways. The polymer therefore exhibits minimal systemic toxicity. PLGA is for instance used in the production of bioresorbable surgical devices [11].

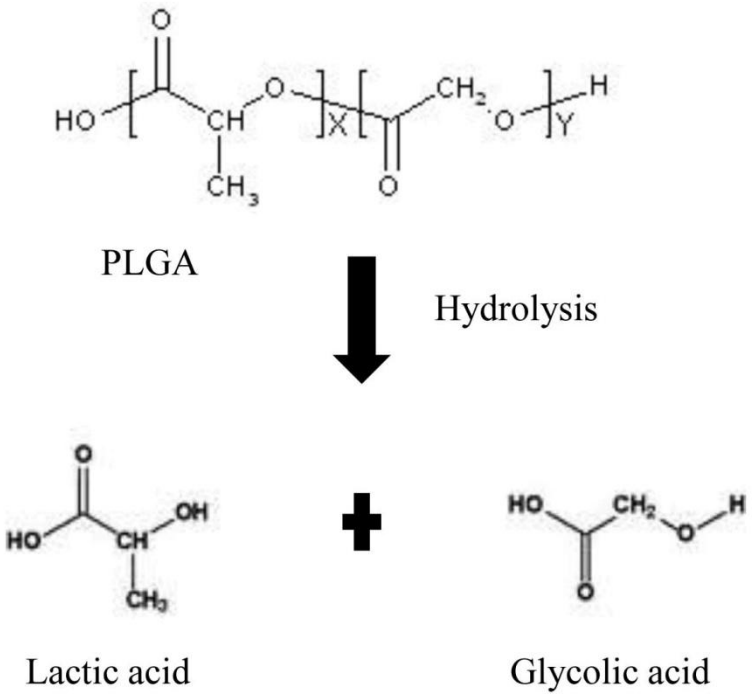

Figure 1.2 *Structure and biodegradation of poly (lactic-co-glycolic acid), PLGA. X and y is the number of lactic acid units and glycolic acid unit, respectively. Modified from [11].*

PLGA polymer properties depend on several parameters. The molecular weight, composition and even the type of drug incorporated play a role. The ratio of lactic to glycolic acid can be varied to produce nanocolloids with tuneable mechanical properties and a wide range of erosion times. The presence of methyl side groups in PLA makes it more hydrophobic than PGA. PLA rich PLGA polymers therefore adsorb less water, and degrade more slowly. The biodegradation of PLGA is directly related to its degree of crystallinity. The crystallinity of the polymer depends on the molecular weight. A high degree of PGA will reduce the PLGA co polymers crystallinity and promote hydration and hydrolysis. Increasing amounts of PGA therefore leads to faster degradation rates, and a ratio of 50:50 of PLA/PGA shows the fastest degradation [11]. The composition of the polymer chosen influences the nanocolloids produced together with many other parameters. If the polymer degradation occurs suddenly with a change in the environment or at a specific time point this might lead to dose dumping, meaning that a large dose meant for sustained release is suddenly released into the environment [18]. Other problems such as inconsistent release and drug-polymer interactions can occur and affect the pharmacokinetics of the nanocolloids [11]. The releases of the drug from the polymer matrix represent a parameter that needs to be carefully investigated.

All nanocolloids show quick clearance from the blood stream und uptake by the mononuclear phagocyte system (MPS) and naked nanocolloids therefore has a relatively poor therapeutic effect [17]. Biodistribution investigations of PLGA nanocolloids have indicated accumulation in tissues such as liver, bone marrow, lymph nodes, spleen and peritoneal macrophages [11]. Their hydrophobic surface makes them easily recognizable for the macrophages in the blood stream. To render the surface of the nanocolloids more hydrophilic, they are often coated with highly hydrophilic molecules such as PEG and polyethylene oxide (PEO). PLGA is often made as a block copolymer together with PEG (Figure 1.2). Both diblock copolymers and triblock copolymers with ABA (PLGA-PEG-PLGA) and BAB (PEG-PLGA-PEG) types exist. In the diblock types the PEG molecules orient themselves towards the exterior of the particle, and provide steric and hydrated repulsion [11]. This comes with the price of reduced drug loading capacity due to steric interference of interactions between PLGA and the drug [11]. As the PEG is bound the PLGA no desorption of the PEG layer can take place.

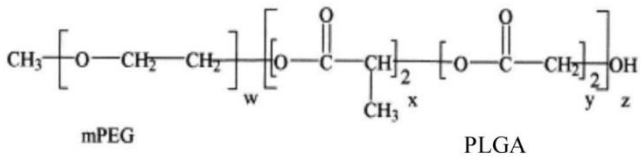

Figure 1.3 *Structure of PLGA-PEG diblock copolymer. X and y represent the number of PLA and PGA monomers, respectively. Y represents the number of PEG monomers present on the diblock polymer.*

For a colloidal system to be stable repulsive forces between the particles in the colloidal dispersion must be dominant to prevent flocculation and coagulation (Figure 1.3). Irreversible droplet size increases leads to destabilisation through two mechanisms, Ostwald ripening and coalescence. Ostwald ripening is growing of the lager droplets at the expense of the smaller ones while coalescence occurs when two drops collide and merge. Coalescence is the main destabilising mechanism in micro sized colloids, but is normally prevented with nanoemulsions due to the small droplet size. Ostwald ripening is therefore process the main nanoemuslion destabilising mechanism [19]. There have been some indication that the trapping of the lipophillic species such as soy lecithin within the oil droplet and polymeric shell of lipid nanocolloids is able to limit Ostwald ripening and aid in the stabilisation of the lipid polymer nanocolloids [19]. The lipid nanocolloids also experience favoured stability due to the heterogeneous nature of the lipid core [20].

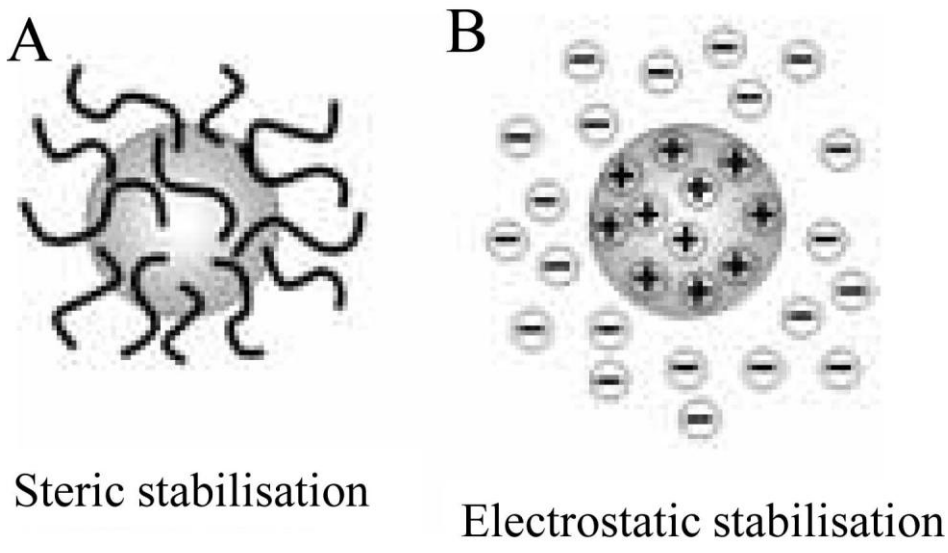

Figure 1.4 *A: Steric stabilisation due to macromolecules such as PEG hindering the particles in close association. B: Electrostatic repulsion due to distribution repulsive mechanisms between particles of equal charge. Modified from [21].*

The zeta potential represents an index for electrostatic stabilization of nanocolloids (Figure 1.4). The zeta potential is a measure of the surface charge of the particle. As the potential increases or decreases the stronger the electrostatic repulsion between particles becomes leading to stabilization. A nanocolloid stabilized solely by electrostatic repulsion needs to have a minimum zeta potential of ± 30 mV [21] Nanocolloids with PEG on the surface normally have a negative zeta potential due to the hydrated layer formed on the surface of the nanocolloids [4]. The PEG chains will give steric repulsion in addition (Figure 1.3), and PEG therefore has a double role in rendering the nanocolloids more stable, aiding in both electrostatic and steric stabilisation.

The most common method for producing PLGA nanocolloids is the solvent evaporation method first described by Fessi, H., *et al.* [22], but others such as the double (multiple) emulsion method, phase separation and salting out of nanocolloids have also been utlised. The main problem when trying to encapsulate a hydrophillic species is the rapid diffusion of the molecule in the outer aqeous phase during emulsification. Therefor a variation of the of the solvent evarporation method was developed, the nanoprecipitation method (Figure 3.1) [23]. In this method the organic solution is added to the aqeous phase in a controlled manner, ie drop-wise or injection by needle [24]. Nanocolloids are formed instantly by rapid solvent diffusion [17]. This method is described in detail in section 3.1.1. Several nanocolloid structures can be produced by these methods, and the terminolgy around the nanocolloids are

sometimes confusing and overlapping. PLGA can form micelles, solid nanoparticles, nanocapsules and polymersomes to name some [3]. Solid nanoparticles (also called nanospheres (Figure 1.1 A) have a solid polymer matrix that drugs can be dissolved, entrapped, encapsuated, cheimically bound or adsorbed to. They are typically between 100 and 200 nm in diameter.The arhitecture of the particles made are strongly dependent on the copolymer composition and moleclar weight of the polymer. Nanocapsules and polymersomes are vesicular systems with the drug entrapped in the core of the nanocolloid. Polymersomes are analogue to liposomes, and have an aqeous core surronded by a bilyaer of the polymer [3]. They are good carriers for water soluble therapeutics. Polymersomes can be sized from 5 nm to 5000 nm. Nanocapsules (Figure 1.1 B) have an oily core and a solid layer of polymer surrounding the core. They have a size range of about 100-300 nm. They therefore have a high volume reservoar for the encapsulation of lipophillic species. Nanocapsules are made with an mixture of polymer and lipids such as soy lechitin. The choise of lipids influcences the visocity of the oily core, and it can be adapted to the viscosity of the lipid cargo [25]. The nanocapsules produced in this study are composed of a mixture of solid and liquid lipids, and the composition of the lipids (soy lechitin and miglyoil) cold be changed to fasilitate the drug that is beeing incorporated.

The drug loading capacity of the nanocolloids and the interactions between the drug and the polymer depend on the chemical structure of the drug, the chemical properties of the polymer chosen and the conditions during drug loading [17]. The biodegradation of these nanocolloids is affected by several parameters such as morphology, porosity, glass transition temperature and additives in the composition. It is difficult to predict the biodistribution of nanocolloids and *in vivo* studies are necessary to evaluate each nanocolloid designed [26].

1.3 Use and potential areas of application for nanocolloids

The use of polymeric nanocolloids holds promises of enhancing drug delivery of a wide variety of therapeutics in several therapeutic areas. Particular in the fields of cancer therapy due to the EPR effect and as controlled delivery devises for vaccines these colloidal drug delivery systems show promising results [4]. Examples of targeting moieties that have been used together with PLGA nanocolloids are folate [27] and specific peptides or carbohydrates that are selective for selectins and integrins [28]. Folate receptors are expressed in several human cancers [29], while selectins and integrins are involved in metastatic events [17].

PLGA lipid nanocolloids have been developed that were labelled with folate. They had the FDA approved NIR dye ICG encapsulated [27]. It was showed that the nanocolloid was actively taken up into cells presenting folate receptors, and through in vivo imaging that the nanocolloids labelled with folate developed higher accumulation into the tumours areas as compared to free dye and non-folate labelled nanocolloid [27]. Jubeli *et al.* developed PLGA nanocolloids to target E-selectin receptors though a well-described glycoprotein. The nanocolloids consisted of PLGA conjugated to PEG that already had been covalently bound to the targeting glycoprotein. In addition the nanocolloid contained a PLGA polymer covalently bound the NIR dye rhodamine (Figure 1.6). These nanocolloids showed promising results *in vivo.* They were shown to be internalised and concentrated in the targeted tissues [28].

Nanocolloids have been used to encapsulate the anti-malaria drug halofantrine. This drug has serious cardiotoxixty, which hinders intravenous administration during the acute phase of malaria. The nanocolloids allowed injection of higher doses and they showed longer circulation times than the free dye and importantly, no cardiac side effects were observed [30].

Polynucleotide, DNA and plasmid vaccines work by delivering genes for expression in host cells, so that the anti-genic protein is produced in the vicinity of professional antigen presenting cells. Both humoral and cell mediated immune responses are initiated. The polynucleotide needs to be delivered to the target cells, internalise to the nucleus, and remain bioactive in the biological environment [17]. Nanocolloids serves as a very promising platform for the delivery of macromolecular vaccines and a lot of research is being conducted in the field.

Interest in oral delivery of nanocolloids, followed by uptake into the Peyer's patches and adjacent lymphoid tissue has been shown a lot of interest, and could aid in the development of oral vaccines and in cancer therapy [4]. PEG has been show to enhance mucoadhesivity in the Peyer's patches [17]. This route has the advantage of avoiding fist pass metabolism that could be advantageous for several therapeutics [31]. Nanoparticles have a large surface area and good mucosal permeation. The lungs have a rich blood supply and thin alveolar walls. This means that nanoparticles could be used in inhalation formulations. Here positively charged PLGA nanocolloids surface coated with chitosan have showed the best results, due to their enhanced mucoadhesivity [4].

Nanocolloids have also been developed for uptake through the blood brain barrier (BBB) via specific receptor mediated uptake [17]. PGLA were conjugated either to a targeting moiety or a NIR fluorescent dye in the Texas red family. Mixtures of these polymers were used produce PLGA nanocolloids that crossed the BBB, and that could be visualized through NIR in vivo imaging [32]. More specific ligands and better surface coating of the polymeric nanocarriers are needed before targeting of the BBB can be effectively achieved.

1.4 NIR optical imaging in the drug development process and as a diagnostic tool.

The drug discovery process is long and expensive and most drugs leads are discarded in the transition between *in vitro* and *in vivo* investigation due to unfavourable pharmacokinetics [14]. The use of nanocolloids could mean that drugs previously discarded can be further developed. NIR imaging can aid in drug discovery in the laboratory, during translation from *in vitro* research to preclinical investigations and eventually in evaluating the biodistribution, pharmacokinetics and biological activity of promising therapeutic agents [14]. Nanocolloids are accumulated in tumour tissue due to the EPR effect, and therefore most of the nanocolloids developed for imaging purposes are designed for cancer research. The use of NIR optical imaging is not as commonly used in humans as MRI.

In animal research one of the main principles are the three R's. This stands for replacement, reduction and refinement. Replacement is difficult, as few systems can mimic the complicated systems experienced *in vivo.* Some has therefore suggested using responsibility as an alternative R [33]. The use of NIR imaging during animal experiments will reduce the amount of animals needed, as the same animal can be tracked over longer periods of time, instead of euthanising animals at each time point. In addition it will lead to refinement of the experiments. Several parameters can be refined. Excitement in the far red window leads to better spatial resolution [14] the incorporation of the fluorophore into nanocolloids leads to better signal to background ratios and quantum yields [34]. More specific limits in the experiments can be set, for parameters such as tumour growth, due to the *in vivo* evaluations.

The use of NIR optical imaging as a diagnostic and drug discovery tool requires effective fluorescent optical probes. Multimodal polymeric nanocolloids are promising as such probes. They can for instance be used as theranostics, containing both a diagnostic probe and a therapeutic compound. QD's or semiconductor nanocrystals display outstanding optical

properties due to a bright and easily controllable emission maxima, and broad absorption spectra [35]. But QD's have potential toxic issues, that might hamper further development for human use [20]. Organic fluorophores are more biocompatible, and one is approved for the use in humans by the FDA, indocyanine green (ICG) [27]. But nontoxic organic fluorophores often suffer from rapid photo bleaching, non-specific adsorption of proteins and rapid degradation [6].

Both QD's [5] and organic fluorophores [20, 27, 28, 30, 32, 36, 37] can be incorporated into PLGA nanocolloids. In this study organic fluorophores with satisfactory biocompatibility have been used. When the fluorophore is incorporated into nanocolloids they are less prone to photobleaching, giving better quantum yields. The nanocolloid shields the fluorophore from the environment preventing degradation, known as the matrix shielding effect [6]. Nanocolloids as fluorescent probes have better signal intensity than the organic fluorophore alone, which makes it possible to trace more weakly expressed targets [14]. Nanocolloids can also hold two or more probes, and in this way the chance of reaching the intended target can be increased [14]. Each nanoparticle can accommodate several fluorescent molecules. The main advantage of incorporating the fluorophore into nanocolloids is the increase in circulation half -life and the increased stability of the signal. Some of the polymeric nanocolloids have shown significant leakage and loss of the fluorophore during circulation. The polymer matrix may not be suitable for providing the matrix shielding effect [1].

Nanocolloids made from PLGA can have the fluorescent dye encapsulated or covalently linked to the PLGA polymer backbone. Both methods are used here. A common strategy for making fluorescent nanoparticles is to incorporate lipophillic dyes into the oily cores of nanocapsules (Figure 1.1 B) [30, 37]. In the present study the long chain dialkylcarbocyanine dyes DiD (Figure 1.5 B) and DiI were incorporated into nanocapsules with an oily core.

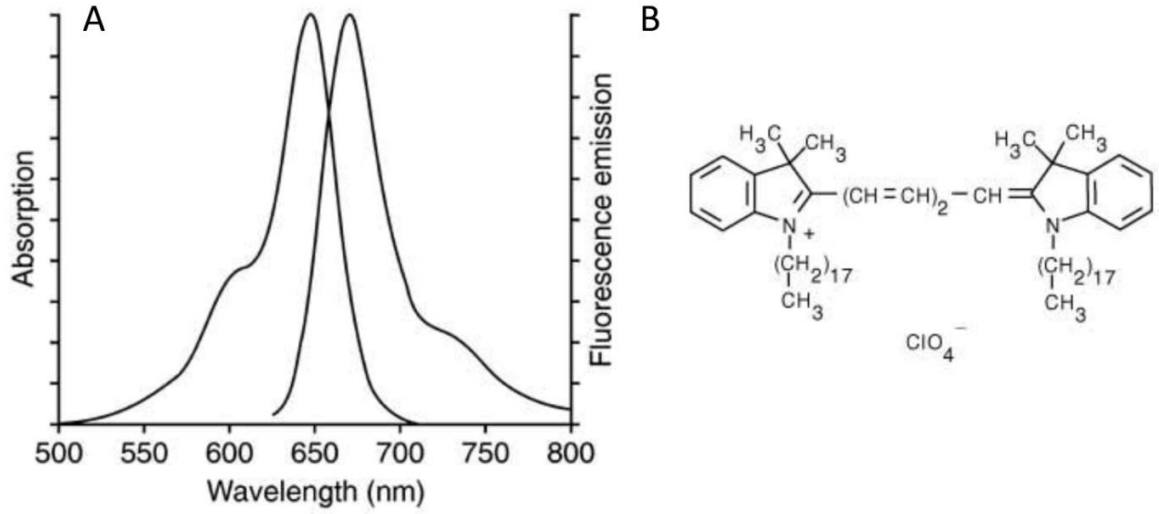

Figure 1.5 *Panel A shows the emission and absorption specter of DiD bound to lipophillic membranes. Panels B shows the molecular structure of DiD. Modified from [38]*

The dyes bind to lipid membranes and are active in the NIR window (Figure 1.5 A). The nonpolar, viscous local environment of nanoemulsions have been shown to promote high quantum yields, 1.6 – 3.2 times higher than their hydrophilic counterpart [20]. These nanoemulsions, also called lipidots by Gravier *et al.*, have shown optical properties that can quantitatively compete with those of commercial QD's. The nanoemulsions also showed low cytotoxicity, and can be used both for *in vitro* and *in vivo* investigations [20]. These "lipidots" were made with the use of high energy ultrasonificaton, to ensure a small particle size. The oily core of the nanocapsules produced here should provide the dyes with a similar environment. Nanocolloids are optically transparent, and during NIR optical imaging we see the fluorophore, and not the nanocolloid itself. There has been indications of swelling and other morphological changes in the dye loaded nanocolloids [6]. This might lead to the dye escaping the nanocolloid, and the advantages of the nanocolloids as contrast agents are lost. The free fluorescent dye can also have different properties when not encapsulated, leading to misinterpretation of results.

In this study solid nanocolloids were also prepared from PLGA covalently linked to two different fluorescent dyes, rhodamine through a PEG spacer (Figure 1.6) [28] and the Texas red dye DY-700 [36]. When the fluorescent dye is covalently linked to the polymer no leakage of the fluorophore is experienced, but smaller amounts are incorporated than when the dye is encapsulated. Due to a more complicated synthesis of fluorescent labelled

polymers, less is known about the differences in biodistribution of nanocolloids consisting of such polymers.

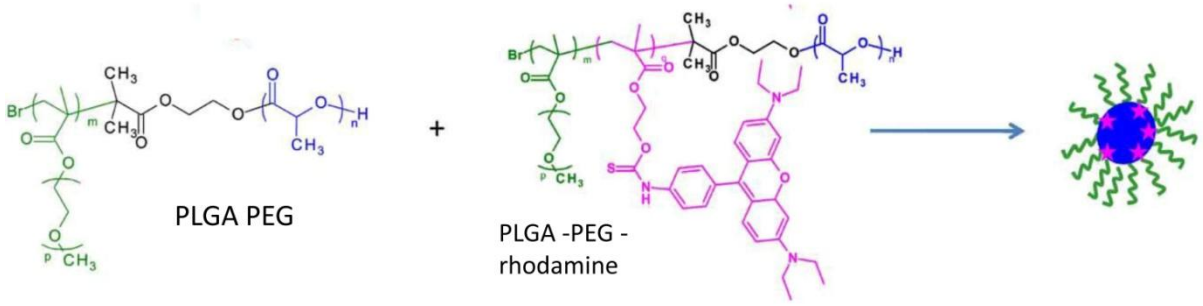

Figure 1.6 *Solid nanoparticles made with PLGA PEG and a PLGA PEG polymer labelled with the fluorescent dye rhodamine. This gives PEGylated fluorescent particles after nanoprecipitation. Modified from reference [28].*

Some evidence of NIR optical imaging in the clinics is emerging. A portable device, the Fluobeam® system uses a laser and a CCC camera in a portable 2D fluorescence system for image guided tumour surgery [14]. As the techniques develop and tissue penetration becomes more efficient NIR optical imaging will play a large role in the diagnostics of tumours and potentially other applications within surgery. The use of PLGA nanocolloids as drug delivery systems will enable the use of drugs previously unattainable due to unfavourable pharmacokinetics and side effects.

1.5 Aims of the study:

The overall aim was to evaluate the biodistributions of fluorescent PLGA nanocolloids, intended to be used as drug carriers for chemotherapeutics. The nanocolloids would be made either as solid nanoparticles with the fluorescent dye conjugated to the polymer or as nanocapsules with an oily core loaded with the fluorescent dye. A mouse model was chosen to conduct in vivo investigations utilizing NIR optical imaging on healthy mice, commonly used to evaluate fluorescent nanocolloids.

The fate of dye-loaded nanocapsules *in vivo* will be evaluated at different time-points, and the effect of PEGylation studied. Analysis the fluorescent lifetimes will be conducted to further evaluate the nature of the fluorescent biodistributions seen. Solid nanoparticles will be evaluated on the biodistribution of the fluorescence, and the effect of PEGylation. The two kinds of nanocolloids will also be compared.

Further *ex vivo* examinations will be conducted to compare with the results seen *in vivo*. No exact quantifications can be done with in vivo imaging, and we wanted to investigate if the results seen *ex vivo* would reflected the distributions seen *in vivo*. The tissue distributions of solid nanocolloids were examined through confocal microscopy.

2. Materials

2.1 Reagents and chemicals

Table 2.1 *Reagents and chemicals:*

Name	Catalogue number	Supplier
Resomer d 50155 (PLGA-PEG)	743423-14-5 (CAS)	Boehringer Ingelheim, Germany
Resomer RG504 (PLGA)	26780-50-7 (CAS)	Evonik Industries, Germany
PLGA-Rhodamine	[28]	A gift from Gillian Barratt, Unv. Paris 11, sud. Chatenay Malabry
PLGA-DY700	[36]	A gift from Nikolas Tsapis, Unv. Paris 11, sud. Chatenay Malabry
Acetone	32201	Sigma Aldrich, USA
Polyvinyl Alcohol (PVA)	P-8136	SIGMA, USA
Sodium Cholate Hydrate	C1254-100G	Sigma Aldrich, USA
Bovine Serum Albumin (BSA)	A-9647	Sigma, USA
VECTASHIELD mounting medium	H-1000	Vector Labs, USA
Tissue Tec o.c.t compound, mounting medium	4583	Sakura Norway AS
Emulmetic (Lecithin) (95 % Phosphatidylcholine)	930	Lucas Meyer Cosmetics, France
Emulmetic (Lecithin) (50 % Phosphatidylcholine)	900	Lucas Meyer Cosmetics, France
Miglyol	810	SASOL Germany GmbH
Sucrose	10274	BDH AnalR, UK
Formaldehyde solution 37 %	1.04003.1000	Merck, Germany
DiD oil (1,1′-Dioctadecyl-3,3,3′,3′-Tetramethylindodicarbocyanine perchlorate)	D307	INVITROGEN™, USA
DiI oil (1,1'-dioctadecyl-3,3,3',3'-tetramethylindocarbocyanine perchlorate)	D282	INVITROGEN™, USA
Sodium dodecyl sulfate (SDS)	L5750-800G	Sigma Aldrich, USA
Peanut oil	315218	A-PRO

All the water used during the experimentation was type 1, reagent-grade water. A Milli-Q Academic water purification system was utilized with a Quantum EX with Millipak-Express 20 Filter unit. During the rest of this text this milli-q water is simply denoted “water”.

2.2 Solutions

1x Phosphate Buffered Saline (PBS), 500 mL

0.1 g KCl,

0.1 g KH_2PO_4

0.675 g $Na_2HPO_4 \cdot 2H_2O$

4 g NaCl, 450 ml water.
The solids were dissolved in the water. The pH was adjusted to 7.4 using 1M NaOH and the volume adjusted to 500 mL. The solution was autoclaved.

2 % v/v formaldehyde in PBS, 500 mL

---

27 mL Formaldehyde solution 37 %

PBS to a total volume of 500 mL

30 % w/v sucrose in PBS, 500 mL

---

150 g Sucrose

PBS to a total volume of 500 mL

5 and 10 % w/v sucrose in water, 100 mL

---

5 or 10 g Sucrose

Water to a total volume of 100 mL

The solution was sterile filtrated through a 0.45 and 0.2 filter

20 % v/w SDS, 500 mL

---

100 g SDS
Water to a total volume of 500 mL

The solution was sterile filtrated through a 0.45 and 0.2 filter

2.3 Mice

BL6, males.		Vivarium
Nod/scid, females.		Vivarium
Housing of animals:		
IVC cage (Green-line)		TECNIPLAST Sealsafe, Italy
Scanbur bedding		Abedd, Germany
Rat and mice no 1 (E)	801002	Special diets services, UK

2.4 Anaesthetics and other drugs

Name	Catalogue nr	Supplier
Isoba Vet (isoflourane, 100 %)	014083	InterVet, The Netherlands
Viscotears	002140	Novartis, Switzerland
Sodium Chloride 9 mg/ml	477786	Fresenius Kabi, Norway.
Hair removal:		
Veet cream (3 min)		Reckitt Benckiser, UK

2.5 Instruments

***Table 2.2**: Instruments with supplier:*

Name:	Supplier:
Laborota 4000 Rotavapor	Heidolph, Germany
PC3001 VARIO$_{PRO}$ vacuum pump	Vacuubrand, Germany
MultiTemp III refrigerated circulator	Pharmacia Biothec, USA.
Zetasizer Nano ZS dynamic light scatterer (DLS).	Malvern Instruments, UK
miniSpin Eppendorf centrifuge	Eppendorf AG, Germany
Sorvall RC 5B pluss centrifuge (Rotor: SS34)	DuPont, USA.
Sonics VibraCell ultrasonicator	Cole-Parmer instruments, USA
Bandelin Sonorex RK 255S ultrasonic bath	Bandelin, Germany
eXplore Optix SAMI LAT optical imaging system	Advanced Research Technologies, Canada
eXplore Optix MX Optical imaging system	Advanced Research Technologies, Canada
In Vivo FX PRO Optical imaging system	Carestream Molecular imaging, USA
Leica CM3050S Cryocutter	Leica, Germany
Varian Cary Eclipse Fluorescence spectrophotometer	Holger, Germany
Test tube rotator (28000)	Lainco BV, The Netherlands
Leica SP2 AOBS confocal microscope	Leica, Germany
Zeiss Apo Tome axioplan 2 fluorescence microscope with a AxioCAM RRM camera	Zeiss, Germany
ChroMini hair clipper	MOSER®, Germany
Isoflourane vaporizer	Harvard apparatus, UK

2.6 Computer software

Name	(use)	Supplier
EXCEL	(statistical analysis)	Microsoft
Graph Pad Prism 5.04	(statistical analysis)	Graph Pad Software Inc
Zetasizer Software	(DLS, zeta potential)	Malvern Instruments
eXplore ArtOptix	(Imaging)	General Healthcare
Carestream MI	(Imaging)	Carestream Molecular imaging
PhotoShop	(Image prosessing)	Adobe
ImageJ	(Image analysis)	U. S. National Institutes of Health

2.7 Disposable consumables

Table 2.3 *Disposable consumables:*

Name	Catalogue number	Supplier
Eppendorf tube, 1,5 mL	7590 15	BRAND
Falcon tubes, 15 mL	188271	CellStar
Falcon tubes, 50 mL	227261	CellStar
Transfer Pipettes	86.1172/86.1173	SARSTEDT, Germany
Scalpels No 11	0303	Swann-Morton, UK
Syringe OmnicanTM 0,5 mL (0,3x12 mm)	9151125	Braun, Germany
Syringe 1 mL BD Plastipak	302187	BD Medical, Spain
Syringe 5 mL BD Plastipak	300013	BD Medical, Spain
Syringe Filter Filtropur 0.45 μm	83.1826	SARSTEDT, Germany
Syringe Filter Filtropur 0.20 μm	83.1826.001	SARSTEDT, Germany
Tubes 13 mL	62.515.006	SARSTEDT, Germany
Glass vials 20 mL		Perkin Elmer®, USA.
Disposable curettes (Size)	7590 15	Brand, Germany
Folded capillary cuvette (Zeta)	DTS 1061	Malvern, UK.

3. Methods

Unless otherwise stated all statistical analysis and data processing was performed in Microsoft EXCEL. All errors are given as standard error of the means.

3.1 Production of solid nanoparticles by the precipitation method:

The particles were made using an adaptation of the nanoprecipitation method [22]. The polymer was first dissolved in acetone and the organic phase was then added drop-wise to the water phase containing a stabiliser (Table 3.1). This was done using a glass syringe with a needle with an inner diameter of 1 mm, while under vigorous stirring to ensure that the acetone was rapidly dispersed in the aqueous phase (Figure 3.1). This gives the particles uniform size. The polymer dissolves in acetone, but not in the water mixture and precipitates in the water/acetone mix. If the particles were to be loaded with a drug, this would also be dissolved in the organic phase. An opaque solution was achieved as the particles were formed. The acetone was then evaporated using a rotavapor. Evaporation of acetone was confirmed by smelling and by measurement of the remaining volume. If this was lower than the volume of water phase in the emulsion it was assumed that all the acetone was removed.

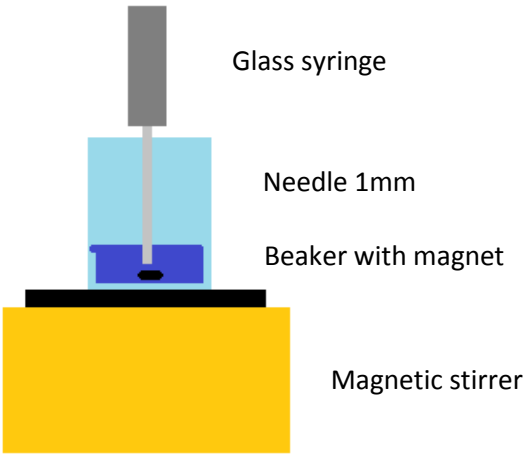

Figure 3.1 Nanoprecipitation by glass syringe. Note that the tip of the needle is below the surface of the water phase.

The nanoparticles were next washed by adding 10 ml water to the emulsion, followed by centrifugation at 20 800 x g for 30 min. The supernatant was removed and the pellet redispersed in water. The particles were then centrifuged for another 30 minutes at 20 800 x g. The supernatant was removed and the particles redispersed in 0.5 ml of 5 % w/v sucrose in water. They were sterile filtrated through a 0.45 µm filter before use and/or injection into animals.

The size and polydispersity of all nanoparticles made were evaluated by dynamic light scattering, DLS (section 3.3.1).

Table 3.1: Solid nanoparticles made by the nanoprecipitation method:

	Organic phase:	Water phase:
PEGylated particles for evaluation. Section 3.1.1	PLGA; Resomer 50155. Stock: 7.5 mg/ml and 2.5 mg/ml. See table 3.2	Polyvinyl alcohol 0.5% w/v, 5 ml.
PEGylated particles for evaluation. Section 3.1.1	PLGA; Resomer 50155. Stock: 7.5 mg/ml and 2.5 mg/ml. 4 ml stock solution added to water phase	Sodium cholate 1.5 % w/v, 5 ml.
PEGylated particles with Rhodamine for in vivo use. Section 3.1.2	7.5 mg PLGA Resomer 50155 7.5 mg PLGA-Rhodamine Dissolved in 4 ml acetone	Sodium cholate, 1.5 % w/v 5 ml.
UnPEGylated particles with Rhodamine for in vivo use. Section 3.1.2	7.5 mg PLGA Resomer RG504 7.5 mg PLGA-Rhodamine. Dissolved in 4 ml acetone	Sodium cholate, 0.5 % w/v 5 ml.
PEGylated particles with DY-700 for in vivo use Section 3.1.2	27.7 mg PLGA Resomer 50155 0.3 mg PLGA-DY 700 Dissolved in 4 ml acetone	Sodium cholate, 0.5 % w/v 5 ml.
UnPEGylated particles with DY-700 for in vivo use. Section 3.1.2	27.7 mg PLGA Resomer RG504 0.3 mg PLGA-DY 700 Dissolved in 4 ml acetone	Sodium cholate, 0.5 % w/v 5 ml.

3.1.1 Production of non-fluorescence solid nanoparticles:

To make particles stabilised by PVA, two stock solutions of polymer in acetone were prepared (Table 3.1 and 3.2). The amount of polymer varies, but the amount of water phase is kept constant at 5 mL. The water phase contained 0.5 % w/v polyvinyl alcohol. They were prepared as described in section 3.1.

Table 3.2 *Nanoparticles prepared to compare the effect on size when varying the amount of polymer.*

Stock solution (mg/mL)	Amount of stock solution (mL)	Amount of PLGA (mg)
7.5	4	30
7.5	3	22.5
7.5	2	15
7.5	1	7.5
2.5	4	10
2.5	3	7.5
2.5	2	5
2.5	1	2.5

To make particles stabilised by sodium cholate, stock solutions of PEGylated PLGA in acetone with concentrations of 2.5 mg/mL and 7.5 mg/mL was made. 4 mL aliquots of these organic phases, equivalent to 10 and 30 mg PLGA, were taken out and precipitated into 5 ml of the water phase as described in section 3.1, see table 3.1. The water phase contained 1.5 % w/v of sodium cholate as the stabiliser.

3.1.2. Solid particles conjugated with a fluorescent moiety for in vivo experimentation:

The particles with rhodamine-conjugated polymer (PLGA-rhodamine) were prepared by dissolving a mixture of PLGA-rhodamine and PLGA with or without PEG at a 1:1 ratio in acetone to reach a final concentration of 3.75 mg/mL. A total of 15 mg polymer is added to 5 mL of 1.5 % w/v sodium cholate. The particles were prepared as described in section 3.1. The polymer conjugated to rhodamine contains short PEG chains (300 g/mol), estimated to be too short to mask the charge of the PLA blocks end-groups of the copolymer [28]. The particles made with unPEGylated PLGA were therefore regarded as unPEGylated.

The unPEGylated particles aggregated during centrifugation, and the aggregate could not be reconstituted. These particles were instead evaporated to a total volume of 1 mL, and then sterile filtrated through a 0.45 um filter. Then they were made isotone by mixing equal amounts of the particle solution and a 10 % w/v sucrose solution. Less of the stabiliser was removed by this procedure, therefore a lower concentration of stabilizer was used, 0.5 % sodium cholate.

The particles with PLGA conjugated to a Texas red dye, DY-700, was made with 0.5 % w/v sodium cholate as the stabilizer. One percent of total polymer was PLGA-DY [36]. A total of 30 mg polymer was dissolved in 4 mL organic phase (Table 3.1). The particles were prepared as described in section 3.1. After precipitation a pale blue opaque emulsion was formed. As for the rhodamine particles, the unPEGylated particles were not centrifuged, but evaporated to a volume total of 1 ml, and sterile filtrated as described for the rhodamine conjugated particles.

3.2 Preparation of nanocapsules with an oily core.

Nanocapsules were prepared using the nanoprecipitation method [22]. The polymer, PLGA with or without PEG, Mygliol as the oily core, soy lecithin as surfactants and either DiD or DiI were dissolved in acetone (Table 3.3). The mixture needed to be heated to about 45 °C to dissolve the soy lecithin. This organic mixture was then added drop-wise to the aqueous phase as shown in Figure 3.1. If the acetone is not rapidly dispensed through the water phase, larger aggregates are formed. No stabilizer was used.

After precipitation the organic solvent was removed by evaporation at 150 bar, using a rotavapor. The pressures was then reduced to 30 bar, and the solution was further

concentrated to a volume of approximately 1 ml. It was then sterile filtrated through a 0.45 µm filter.

Table 3.3: *Nanocapsules prepared:*

	Organic phase:	Water phase:
Empty PEGylated nanocapsules for characterization:	In 10 ml of acetone: 15 mg PLGA: Resomer 50155 62,5 uL Mygliol 9,375 mg Emulmetic 930 9,375 mg Emulmetic 900	5 ml water
DiD loaded PEGylated and unPEGylated nanocapsules for NIR imaging.	In 10 ml of acetone: 15 mg PLGA: Resomer 50155 in PEGylated, Resomer RG504 for unPEGylated. 3mg DiD 62,5 uL Mygliol 9,375 mg Emulmetic 930 9,375 mg Emulmetic 900	5 mL water
DiI loaded PEGylated and unPEGylated nanoparticles for NIR imaging	In 10 ml of acetone: 15 mg PLGA: Resomer 50155 for PEGylated, Resomer RG504 for unPEGylated. 1 mg DiI 62,5 uL Mygliol 9,375 mg Emulmetic 930 9,375 mg Emulmetic 900	5 mL water

Before in vivo use the nanocapsule suspension was adjusted to isotonic 5 % sucrose by mixing 1:1 with 10 % w/v sucrose solution.

All particles made were evaluated for size and polydispersity by DLS, see section 3.3.1

3.3 Characterisation of nanocolloids

3.3.1 Dynamic light scattering, DLS:

To evaluate the size, polydispersity and zeta potentials of the nanocolloids, a Zetasizer Nano ZS DLS was used. This measures the Brownian motions of the nanocolloids, and uses this and the given viscosity of the dispersant to calculate the size of a sphere that would move with the same speed as the nanocolloid in the sample. One will thus get information about the hydrodynamic diameter and the polydispersity of the nanocolloids in the suspension.

All measurements were done at a 1:100 dilution of nanocolloid solution in water. The contents were thoroughly mixed, and transferred to disposable plastic cuvettes. PLGA was chosen as the material and water as the dispersant. The Zetasizer Nano ZS optimises measurements settings to obtain reliable measurements. Each sample was measured three times, and data was given as z-average (nm, diameter), PDI (Mw/Mn) and peak size (nm, diameter).

To evaluate the zeta potential of the different nanoparticles, the samples were diluted 1:100 in water and transferred to a Malvern folded capillary cuvette, making sure there was no air in the loop. The system was set to make between 10 and 500 measurements in each run, and three runs were made on each sample. The zeta potential is a measurement of electric potential in the interfacial double layer of the particles, the potential difference between the dispersion medium and the stationary layer of fluid attached to the dispersed particle (Figure 1.4).

3.3.2 Evaluation of binding to bovine serum albumin, BSA:

Measurements were preformed as described in section 3.3.1. First the size of BSA was measured at 0.3 mg/ml. Next, nanocolloids were measured, and BSA then was added to a final concentration of 2.73 mg/ml BSA.

Nanocolloids, that had been stored at 4°C for 1-3 months, were suspended in isotone 5 % w/v sucrose. They were first measured before BSA was added. A 1:100 dilution of the colloids in water were used for these measurements. The samples with nanocolloids and BSA were measured after 15 minutes and 3 hours of incubation while shaking.

3.4 Mouse handling.

The mice used in this study were Nod/Scid and BL6 strains. All animals, approximately 6 weeks of age, were required from Vivarium at UiB and left to acclimatize at BBB, at the University of Bergen for at least 7 days. The study was approved by the local animal welfare comity (number: 2011-3860) and conducted according to the Norwegian Animal Welfare Act. The conductor has completed a course in Laboratory Animal science. The course is according the Norwegian Ministry of Agriculture`s definition of competence as FELASA C researcher.

All animals used were housed in a specific pathogen free environment, a temperature of 21 °C, 50 % relative humidity and 12 hour light/dark cycles. Food and water was available ad

libitum. The food was removed 12 hours before imaging of the animals to avoid autofluorescence from food in the intestine.

To avoid transfer of pathogens between immune-competent and immune-deficient mouse strains, the equipment was always washed thoroughly and sterilised with alcohol before and after use.

3.4.1 Shaving

To avoid autofluorescence from the fur of the mice, the mice were shaved and the hair further removed by applying hair removal cream one week before imaging. The use of the hair removal cream was repeated on the day or the day before the imaging. In this way any nips and cuts would heal. Coagulated blood species in nips and cuts turn up as bright spots on the imaging system, as they have strong autofluorescence. The mice were anaesthetised as described in section 3.4.3. While under anaesthesia the mice were carefully shaved using a hair clipper. The hair removal cream was then carefully distributed on the mouse and left to work for one min. A cotton pad was soaked in tempered water and used to rinse off the cream. When all visible cream was removed the mouse was rinsed again with a clean cotton pad. The mice were then transferred to a solitary chamber to recover from the anaesthesia.

3.4.2 Intravenous (i.v.) injections

Intravenous injection was done on wake mice by placing the mouse in a restrainer. The restrainer has a light source that illuminates the tail from underneath, making the veins visible. The injections were given with a 0.5 mL syringe with a 0.3x12 mm tip.

3.4.3 Sedation

Isoflourane (Isoba Vet^{TM}) was used both to induce anaesthesia, and as a sedative during the procedures. A portable vaporizer system was used to administer the gas. O_2 was used as the propellant gas. The mouse was first put in a chamber until anaesthesia was induced, and then moved to a nozzle either inside the imager or on the table top. The amount of isoflourane administer was lowered to the minimum concentration to keep the animals sedated and the sedation period was kept as short as possible. The mice were put under a heating lamp when recovering from sedation. In addition the mice were given a drop of Viscotears on the eyes when in the imager.

3.4.4 Animal welfare

During the imaging procedure the animals were starved. In some periods the animals also received anaesthetic gas for periods up to 30 minutes. In some instances when the animals appeared to have reduced general condition or recovered poorly from anaesthesia, they would be given either 9 mg/mL sodium chloride or 5 % sucrose by subcutaneous injection.

3.4.5 Euthanasia of mice and collection of organs.

Mice were euthanized by CO_2, and left in the CO_2 chamber for 3 minutes before organs were removed. The abdomen was opened, and white adipose tissue was collected. Next the intestine was removed, and the stomach discarded. The spleen and kidneys were then exposed, and collected, before the liver was pulled away from the diaphragm and cut out. The diaphragm and the ribcage were then opened and the heart and lungs were collected. As much as possible of the muscle was removed from the femurs, and the femur carefully released from the hip bone and after imaging the bone marrow was collected as described in section 3.6.4. Finally, subcutaneous brown adipose tissue was collected from the area between the shoulder blades. A piece of skin from the mice was also collected.

The tissues were imaged as described in sections 3.5.2 and 3.5.3, or processed for cryosectioning as described in section 3.6.2.

3.5 In vivo investigation of nanocolloids

3.5.1 NIR imaging of mice injected with dye loaded nanocapsules

An eXplore Optix from General Healthcare (GH) was used to obtain fluorescent images from the mice injected with nanoparticles loaded with NIR-dye. The mice (female Nod/Scid of 6-8 weeks) were prepared as described in section 3.4.1. A 670 nm laser was utilized with Cy5.5 fluorescence. Emission was measured with a broad field collection filter. The system ran a power automation program to determine the optimal laser power. Scans were recorded at 10 min, 1, 2, 4, 8, 12 and 24 hours. The maximum fluorescence was measured at each time point. After the 24 hours scan, the mouse was euthanized and organs collected as described in section 3.6.1. The organs were placed on white bench paper and photographed before imaging. After imaging bone marrow was collected as described in section 3.6.4.

The injections of nanocapsules given contained 0.275 µmoles of DiD or 0.174 µmoles of DiI. One mouse was injected intravenously (Section 3.4.2) with an equivalent amount of free DiD

dye, and imaged as described. The free dye was dissolved in a small amount of pharmaceutical grade peanut oil, and added isotone sucrose at a ratio of 1:100. This solution was emulsified by a cycle of 10 minutes in an ultrasonic baht followed by 1 minute ultrasonification on a Sonics VibraCell ultrasonicator at 80 amplitude. This was repeated three times.

The fluorescence intensity (photons/second) is then measured. Measurements were made on pixels that were 1.5 mm^2. This is overlaid on a black and white picture of the mouse. Using the software ArtOptix, regions of interest (ROI) of equal size were made at each time point. The amount of fluorescence at in each area of interest was given. Background fluorescence is subtracted from each ROI before analysis. Data analysis, time course graphs and statistical analysis were done in the Prism software. In addition representations of fluorescence lifetime in each pixels were made in the ArtOptix software, along with analysis of the different lifetimes. Due to technical problems with the laser, it was not possible to obtain data for quantification of the imaging of mice injected with the DiI-loaded nanoparticles. One set of pictures is given to exemplify the biodistribution for these capsules.

3.5.2 NIR imaging of mice injected with solid nanoparticles labelled with DY-700:

Female white nod/scid mice, approximately 10 weeks of age, with the fur removed (see section 3.4.1) were used. Before and during imaging they were anaesthetised as described in section 3.3.3. Imaging was performed by a Carestream FXPRO imaging system with x-ray. Excitation was at 710 nm and emission was collected at 750 nm. The animals were imaged at the time-points described in section 3.5.1. The maximum fluorescence was measured at each time point, in addition a white light picture, a fluorescence scan and an x-ray picture was obtained. After the 24 hours scan, the mice was euthanized and organs collected as described in section 3.6.1. The organs of interest were then imaged on a Petri dish. After imaging, the bone marrow was collected from the femur and analyzed as described in section 3.6.4.

Using the imager software overlays of x-ray and fluorescent images were made. In addition regions of interest were drawn on the fluorescent images, and the sum of florescence at each time point collected. The data was normalised for size of the ROIs. These data were used for time course analysis using Prism and is presented together with the images.

3.5.3 Ex vivo imaging of mice injected with solid nanoparticles labelled with Rhodamine:

Male black BL6 mice were used for the in vivo experiments. The particles were administrated as described in section 3.4.2. Twenty-four hours after injection, the mice were euthanized and the organs of interest were removed by dissection as described in section 3.4.5. The specimens were then fixed and cryosectioned as described in section 3.6.1.

The sections were examined by fluorescence microscopy and evaluated for further confocal microscopy (Section 3.6.2). Routinely, fluorescence images were collected (red, green and blue fluorescence) and a visible light image was captured. Based on the fluorescence images, the three best specimens from each organ were chosen for confocal imaging.

3.6 Preparation of mouse specimens.

3.6.1 Fixation of tissues and cryosectioning:

Organs and tissues were fixed in 2 % v/w formaldehyde in PBS for 24-48 hours. The organs were next placed in 30 % v/w Sucrose in PBS until subsidence (Approximately 48-72 hours). This is a sign that they were saturated with sucrose, which serves as a cryoprotectant. The specimens were then transferred to plastic vials with paper in the bottom, and frozen at -80 ^{o}C for at least 24 hours before cryosectioning.

The specimens were kept on dry ice during preparation of cryosectioning. The specimens were fixed to the sample holder using Cytofix^{TM}, and the specimen was then covered with cytofix to ensure maximum rigidity during sectioning. The sample holder with the specimen mounted was left on the dry ice until the fixative had solidified. Cryosectioning was performed at – 20 °C, and sections with a thickness of 14 µm were made. Sections were transferred gently to water and next onto a glass slide. Sections were sampled every 150 µm. The sections were left to dry at room temperature, in the dark, over night. Brown and white adipose tissue sections were not spread on water, as it forms droplets immediately. Instead these sections were placed directly on a room tempered glass slide.

The slides were mounted under cover slips by adding 7 µL of Vectashield ^{TM} onto the sections. This mounting media is glycerol-based and do not solidify, but remains a viscous liquid [39]. It prevents photo bleaching, and is compatible with fluorescence microscopy. Any air bubbles formed under the glass was carefully pushed out and the cover slips were permanently sealed around the perimeter with nail polish. Mounted slides were stored at 4 °C.

3.6.2 Confocal microscopy investigations of solid nanoparticles conjugated with rhodamine.

The sections chosen from the fluorescence microscopy (Section 3.5.1) were evaluated on a Leica SP2 AOBS, and the best section was found for each organ. An HCX PL APO 63.0x1.4 NA oil objective was used. Background fluorescence was gathered by excitation with a 405 nm laser and the emission was gathered between 407 and 478 nm. This channel is portrayed as red. The particles were exited with a 543 nm laser and emission gathered between 550 and 655 nm. This channel was depicted green to facilitate visualisation on the computer screen. The images were recorded in 1024 x 1024 pixels (voxel size of 232 nm) and optimized with two-line averaging. An overlay of the two fluorescent channels red and green was made using Leica Lite software. The confocal imaging was performed at the Molecular Imaging Centre (FUGE, Norwegian Research Council), University of Bergen.

The green channel, depicting the particles, was then processed in Image J, and estimations of positive cells in the sections were made. A cut out value of 4 pixels (about 17 μm^2) was chosen. Four images from different parts of each section were analyzed.

3.6.3 Measurements of fluorescence in bone marrow

The femurs were cut at both ends, and 0.5 mL of PBS was used to flush out the bone marrow repeatedly from the bone. After collection 250 µL of 20 % sterile filtrated Sodium dodecyl sulphate, SDS, solution was added to the total of one mL of bone marrow cell sample for each mouse, to give an end concentration of 5 % SDS. The sample was next centrifuged at 6700 x g for 10 minutes in a miniSpin Eppendorf centrifuge. The supernatant was then transferred to a quarts cuvette for measurements in a Varian Cary Eclipse Fluorescence spectrophotometer. A scan of excitation and emission wavelengths were preformed on DiD and DiI to get optimal signal form the samples. 5 % SDS in water was blank. Six measurements were taken from each sample.

4. Results

4.1 Production and characterisation of nanocolloids made by the nanoprecipitation method.

4.1.1 Solid nanoparticles:

First it was examined if the type of stabiliser could influence the size of the nanoparticles. When the carriers were made with PVA as the stabiliser, the z average size was between 90 and 140 nm (diameter), there was always only one peak, and the polydispersity was below 0.1, which is satisfactory. As the ratio of organic phase to aqueous phase increased, there was an increase in size of the particles (Figure 4.3 A). A ratio of 1:10 organic phase:aqueous phase gave the smallest particles. However, the variations in size were seen under the different conditions tested were small (Figure 4.2). Nanocolloids made with PVA as the stabiliser was difficult to redisperse after centrifugation. In addition it is believed that some PVA remains associated with the nanocarriers despite repeated washing because PVA forms an interconnected network with the polymer at the interface. This is shown to affect the release of the drug load [2].

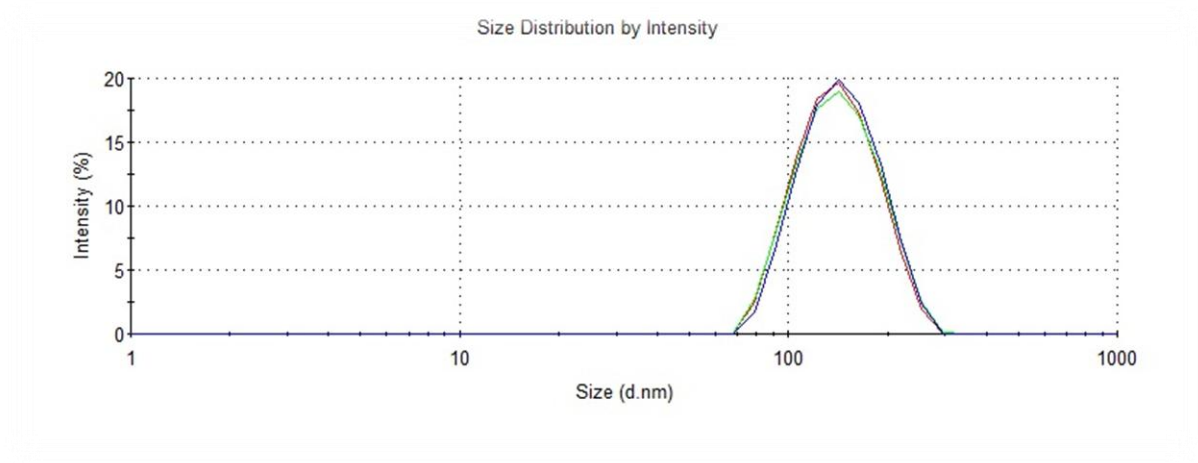

Figure 4.1 *Z-average size (Mw/Mn) for solid nanoparticles made with PVA as the stabiliser and a total of 15 mg PLGA (Ratio organic to aqueous phase: 1:5).*

It was therefore decided to make nanoparticles with sodium cholate as the stabiliser. This is a biocompatible bile salt. When particles were made with sodium cholate as the stabiliser, the particles were smaller than the particles made with PVA, between 55 and 65 nm in z average

diameter (Figure 4.3 B). They also gave pellets that easily redispersed. During the washing cycle the carriers would aggregate if redispersed in PBS. It was therefore decided to redisperse them in isotone sucrose, 5 % w/v, which gave stable pellets that easily redispersed. An example of the size distribution is shown in figure 4.2. Only one peak was seen, and the PDI was low (0.089), although somewhat larger than for the particles made with PVA (0.047).

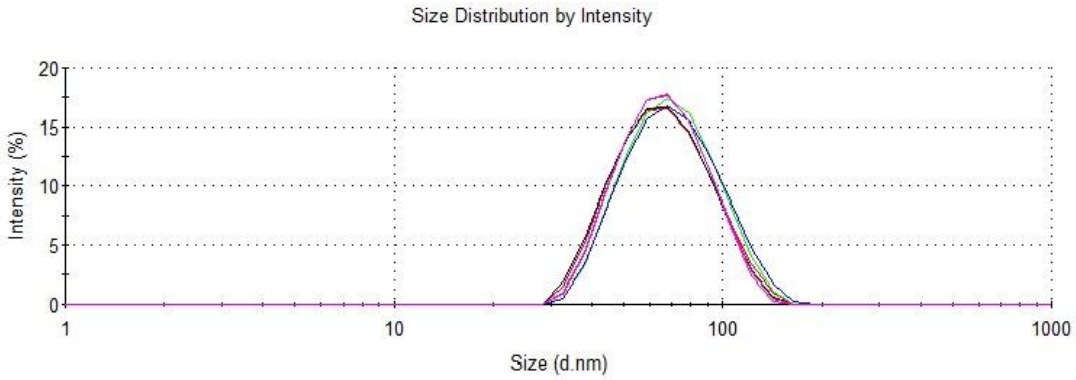

Figure 4.2 *Z-average distributions (Mw/Mn) for solid nanoparticles made with sodium cholate as the stabiliser and a total of 30 mg PLGA (Ratio organic to aqueous phase: 2:5).*

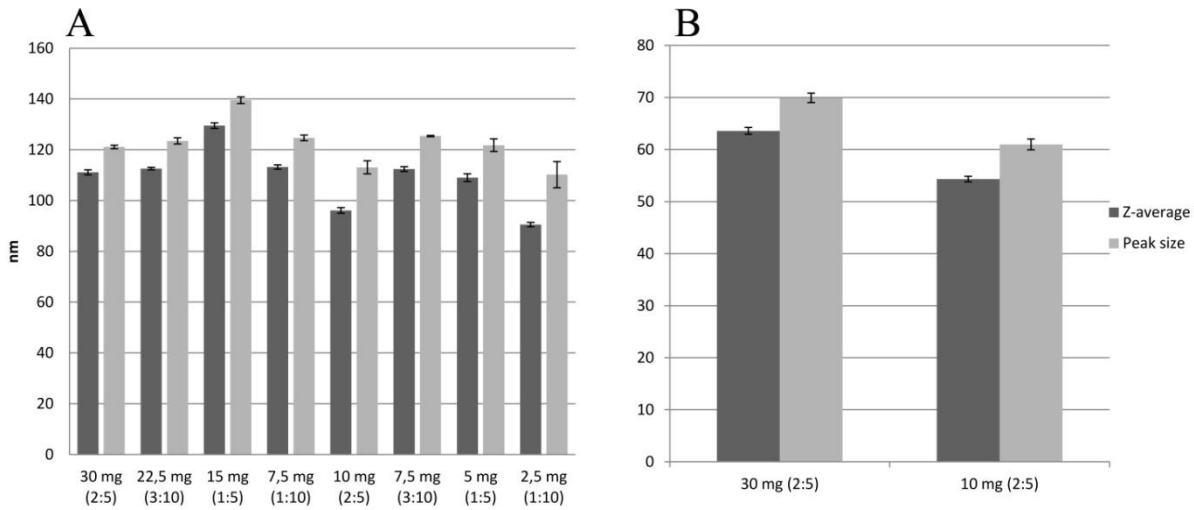

Figure 4.3: *Size of solid nanoparticles made by the precipitation method as described in section 3.1. The amount (mg) of polymer is given together with the ratio of organic phase:aqueous phase, in brackets. Both z-average size and peak size are given. A: Particles made with PVA as the stabiliser. B: Particles made with Sodium Cholate as the stabiliser.*

Based on these results it was decided to continue with a ratio of 2:5 between organic phase and water phase and using sodium cholate as the stabiliser (Table 4.1). The zeta potential of

the different solid nanocolloids produced was next investigated. All the particles had a negative zeta potential (Table 4.1) and the unPEGylated particles showed the lowest potentials, and should experience electrostatic repulsion between the particles, and some degree of electrostatic stabilisation (Figure 1.4).

Table 4.1 *Characterisation of solid nanoparticles conjugated to a fluorescent dye, made for in vivo investigations. The data show average and standard deviation of the mean. Batch to batch variations were under 3 %.*

Nanocolloid	Z average (nm)	PDI (Mw/Mn)	Peak size (nm)	Zeta potential (mV)
PEGylated solid nanoparticles conjugated with Rhodamine	129.9 ± 0.67	0.145 ± 0.004	136.9 ± 1.11	-45.23 ± 4,98
unPEGylated solid nanoparticles conjugated with Rhodamine	133.8 ± 0.92	0.121 ± 0.007	153.7 ± 2.66	Not estimated
PEGylated solid nanoparticles conjugated with DY-700	106.0 ± 0,72	0.254 ± 0,039	108.3 ± 4.66	-22.83 ± 1,17
unPEGylated solid nanoparticles conjugated with DY-700	128.2 ± 5.36	0.123 ± 0,005	142.9 ± 5.64	-52.90 ± 0.88

4.1.2 Nanocapsules with an oily core:

Nanocapsules made by precipitation can be made with or without stabilisator [19, 20, 30, 32].Stabilisation should be enabled though a mixture of the insoluble phospholipids and by steric stabilisation due to the PEGylation [20].

Nanocapsules with a size between 150 and 205 nm were produced. Batch to batch variations were always under 6 %. The polydispersity indexes (Table 4.2) were low and consequently increased as sucrose was added. An example of the size distribution of the nanocapsules is given in Figure 4.4. Both the PEGylated and the unPEGylated nanocapsules show larger size distributions than the solid nanoparticles. The zeta potential of nanocapsules loaded with DiD was investigated (Table 4.2). The nanocapsules showed negative zeta potentials that would give the emulsions some degree of electrostatic stabilisation. As for the solid nanocolloids, the unPEGylated nanocapsules showed the greatest zeta potentials (compared to the PEGylated equivalents). This could indicate that the PEG-chains mask some of the negative carboxyl

groups on PLGA. The zeta potentials are generally higher than the potential measured for the solid nanoparticles (Table 4.1)

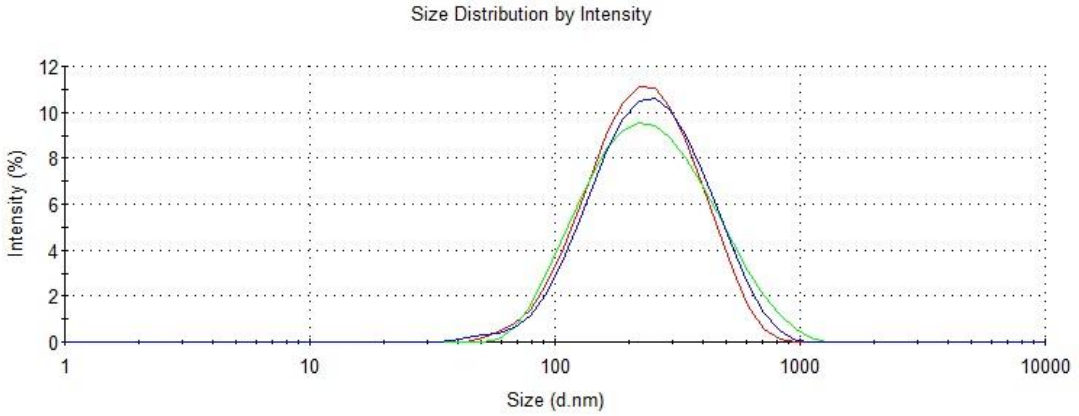

Figure 4.4 *Z-average distributions (Mw/Mn) for unPEGylated nanocapsules with an oily core.*

The stability of the nanocapsules over a month was investigated (Figure 4.5). Nanocapsule suspensions were suspended in 5 % sucrose or in water. The suspensions were then sterile filtrated through 0.45 µm filters and stored in room temperature. Measurements were performed as described in section 3.3.1. The initial size of the capsules was 275.8 ± 9.7 nm. After 7 days the nanocapsules stored in water had decreased in size from 276 nm to about 190 nm and stabilised there. The nanocapsules stored in sucrose showed an increase in size.

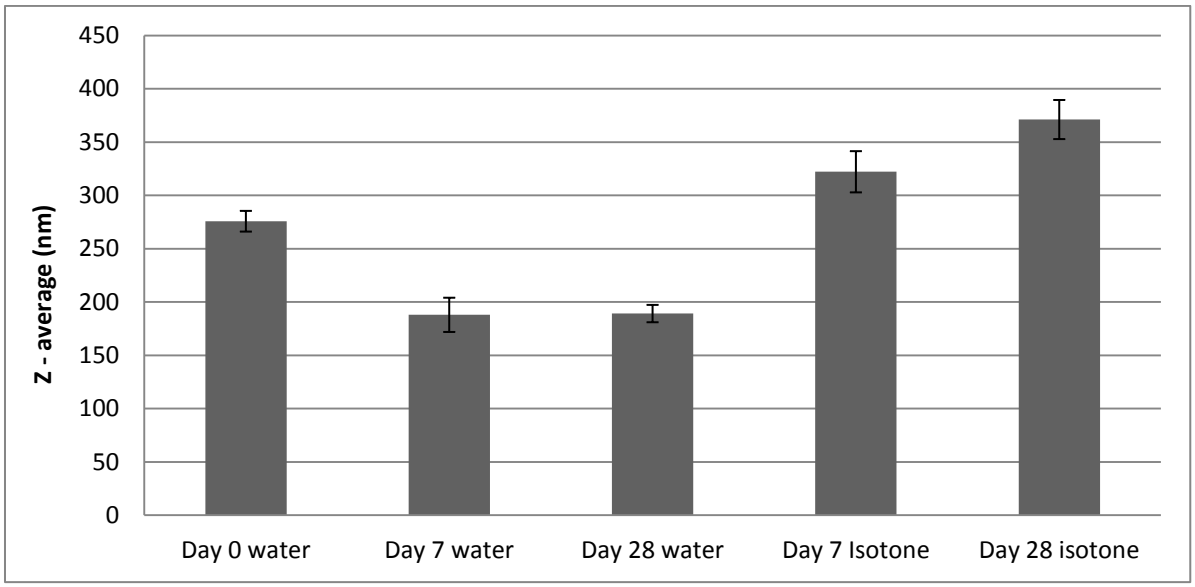

Figure 4.5 *Stability of oily core nanocarriers over one month. They were stored in room temperature either as a sterile filtrate or as an isotone solution. Measurements were made on day seven and 28. The size is given as the z-average (Mw/Mn).*

Table 4.2 *Overview of nanocapsules with an oily core made for in vivo experimentation. The data show average and standard deviation of the mean. Batch to batch variations were under 4 %.*

Nanocolloid	Z average (nm)	PDI (Mw/Mn)	Peak size (nm)	Zeta potential (mV)
PEGylated Nanocapsules with an oily core loaded with DiD	230.4 ± 15.81	0.337 ± 0.022	197.6 ± 14.82	-32.00 ± 2.29
unPEGylated nanocapsules with an oily core loaded with DiD	158.7 ± 0.92	0.203 ± 0.007	154.4 ± 3.54	-22.13 ± 1.31
PEGylated nanocapsules with an oily core loaded with DiI	158.7 ± 2,65	0.261 ± 0.027	154.4 ± 3.54	Not estimated
unPEGylated nanocapsules with an oily core loaded with DiI	189.7 ± 2.31	0.233 ± 0.011	232.9 ± 4.21	Not estimated

4.1.3 Binding of nanocolloids to bovine serum albumin

When foreign bodies are administered intravenously, they are normally cleared form the bloodstream quickly by the mononuclear phagocyte system. If plasma proteins, such as albumin, bind to the nanocolloids this would lead to quicker complement activation and uptake by macrophages. It was therefore decided to investigate if bovine serum albumin (BSA) was adsorbed onto the nanocolloids. BSA was measured as a 0.3 mg/ml solution. The

average size measured were 13.69 ± 5.24 nm. The solution was very polydisperse (0,623 ± 0,282) and two additional peaks at about 50 and 250 nm, probably aggregates, were also seen.

The solid nanocarriers show little variation over the three hours (Figure 4.6 A). The PEGylated nanocarriers showed an increase in size after 15 minutes, and then returned to the original size. This increase was only seen on the first three measurements (Peak size: 130.9 ± 8.15 nm). In the second set of measurements no such increase is seen (Peaks size: 98.0 ± 1.73 nm). The unPEGylated carriers show no variation in size at all, but remain stable at around 160 nm.

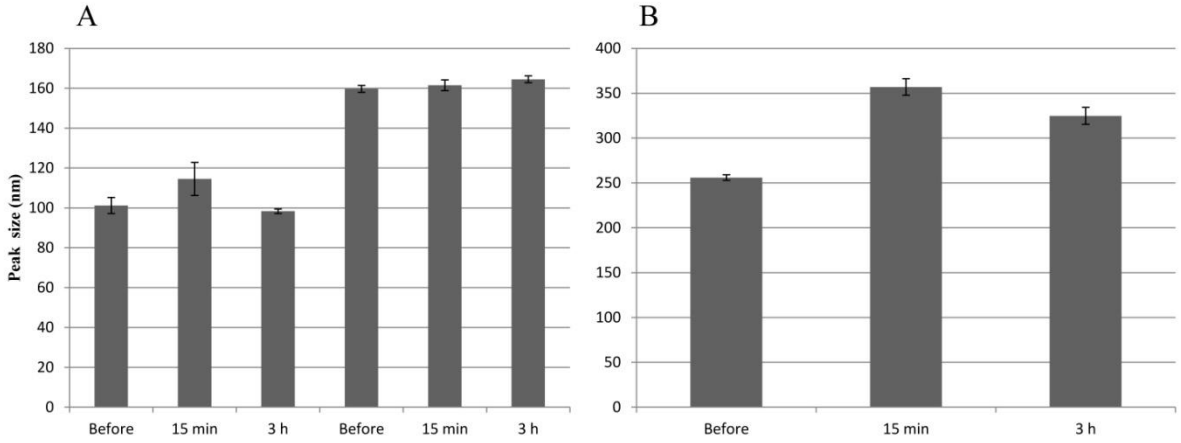

Figure 4.6 *Evaluation of binding to BSA. Measurements were preformed before addition of BSA and after 15 minutes and three hours. A: Comparison of PEGylated and unPEGylated solid nanocarriers. B: PEGylated nanocapsules with an oily core.*

PEGylated oily core nanocapsules increased in size when incubated with BSA, about 100 nm already after 15 minutes (Figure 4.6 B). The size had decreased somewhat again after three hours (324.8 ± 9.46 nm). The same batches of carriers were evaluated at two different occasions, and the mean of 6 measurements is given.

4.2 In vivo distributions of labelled nanocolloids

4.2.1. Biodistribution of nanocapsules with an oily core

We wanted to see the change in biodistribution of nanocolloids over time, and used live imaging to make it possible to follow the nanocolloids in mice in a non invasive manner without sacrificing the animals at each time point. The fluorescence biodistributions of the PEGylated nanocapsules (Figure 4.7 A) showed four main distributions, in areas corresponding to the intestinal tract, liver, lungs and bone. The first four hours there was a

strong signal from liver and lung indicating particles circulating in the blood. The areas around the femurs also showed accumulation of fluorescence at the first time-points. The fluorescence in the organs after 24 hours showed a similar accumulation. (Figure 4.7 B and C). Accumulation of fluorescence in the spinal column and sternum appeared at about 4 hours and then increased over the 24 hours. The femurs were visible from 10 minutes. The development of total fluorescence intensity is shown in Figure 4.7 D. The highest intensity was seen after 10 hours and there was a clear drop after 1 hour. The fluorescence then slowly increases again over the 24 hours. The high readings after 10 minutes (see also 4.8 D) might be due to the particles being highly concentrated in a small area just after injection. Within one hour the nanocapsules might be distributed deeper in the body, which will give lower readings.

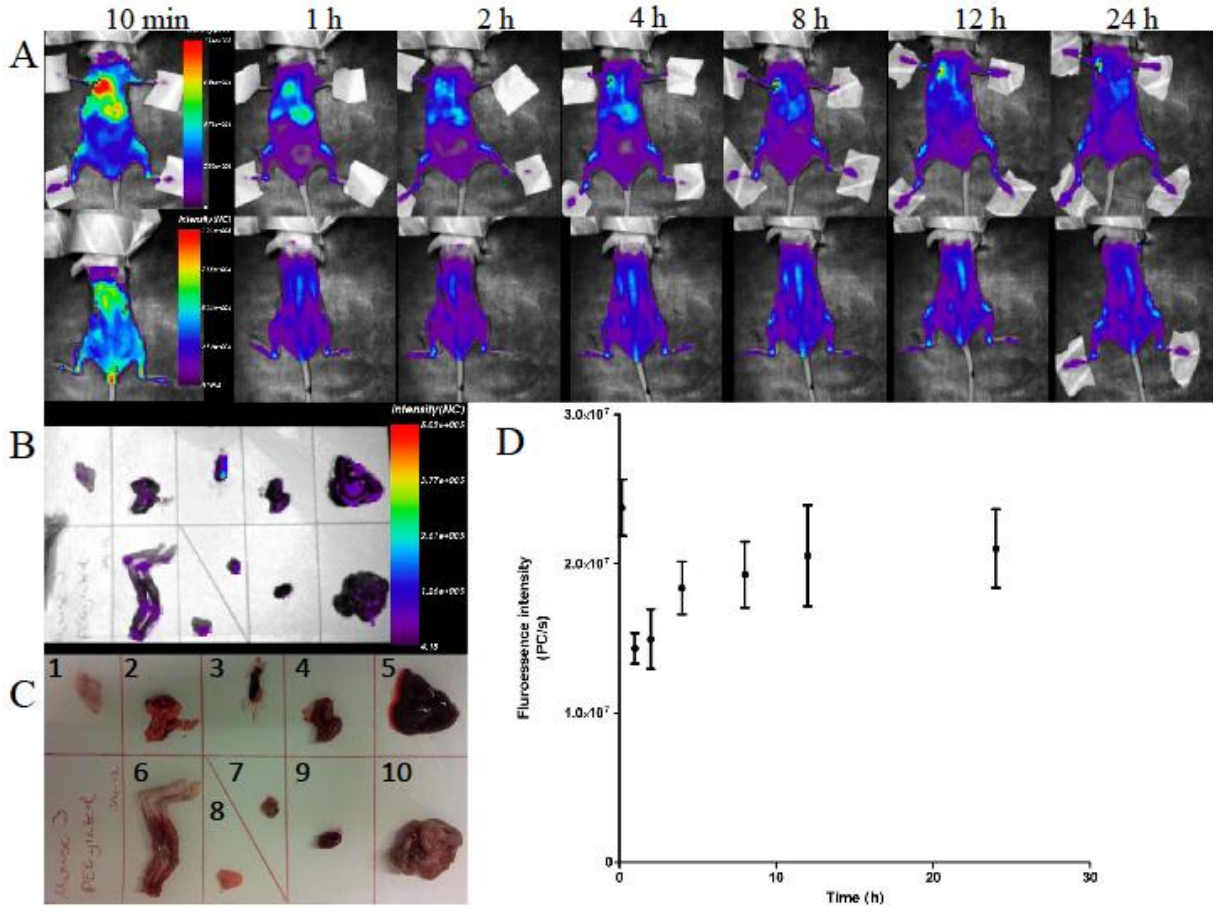

Figure 4.7 *Biodistribution of PEGylated nanocapsules loaded with DiD. A: Fluorescence intensity (photon counts per second) overlaid on an image of the mouse. Ventral and dorsal intensity is shown. B: Fluorescence counts from the organs. C: Colour image of organs scanned.1: Skin, 2: Lungs, 3: Spleen, 4: Kidneys, 5: Liver, 6: Hind legs, 7: Brown adipose tissue, 8: White adipose tissue, 9: Heart, 10: Intestine D: Development of the fluorescence intensity over 24 hours. Ventral and dorsal maximum fluorescence is added at each time point (6 measurements).*

The unPEGylated nanocapsules showed a similar fluorescence biodistribution to the PEGylated nanocapsules (Figure 4.8). Fluorescence from the femur area developed more slowly than for the PEGylated nanocapsules but a clear uptake was seen (Figure 4.8 A). The signal from the liver stayed more consistent over the 24 hours than it did in the mice given PEGylated capsules. Lower initial and overall fluorescence intensity was seen for these capsules (Figure 4.8 D). The strongest intensity for these capsules was seen after 12 hours. There was an initial drop, but it is not as marked as for the unPEGylated capsules. The organs showed a similar distribution what was seen during the *in vivo* imaging, with strong fluorescence from liver, spleen and adipose tissues, in addition to the intestine (Figure 4.8 B and C). More fluorescence from the lungs and liver was seen for the unPEGylated nanocapsules (Figure 4.7 C and D) than for the PEGylated nanocapsules (Figure 4.8 C and D).

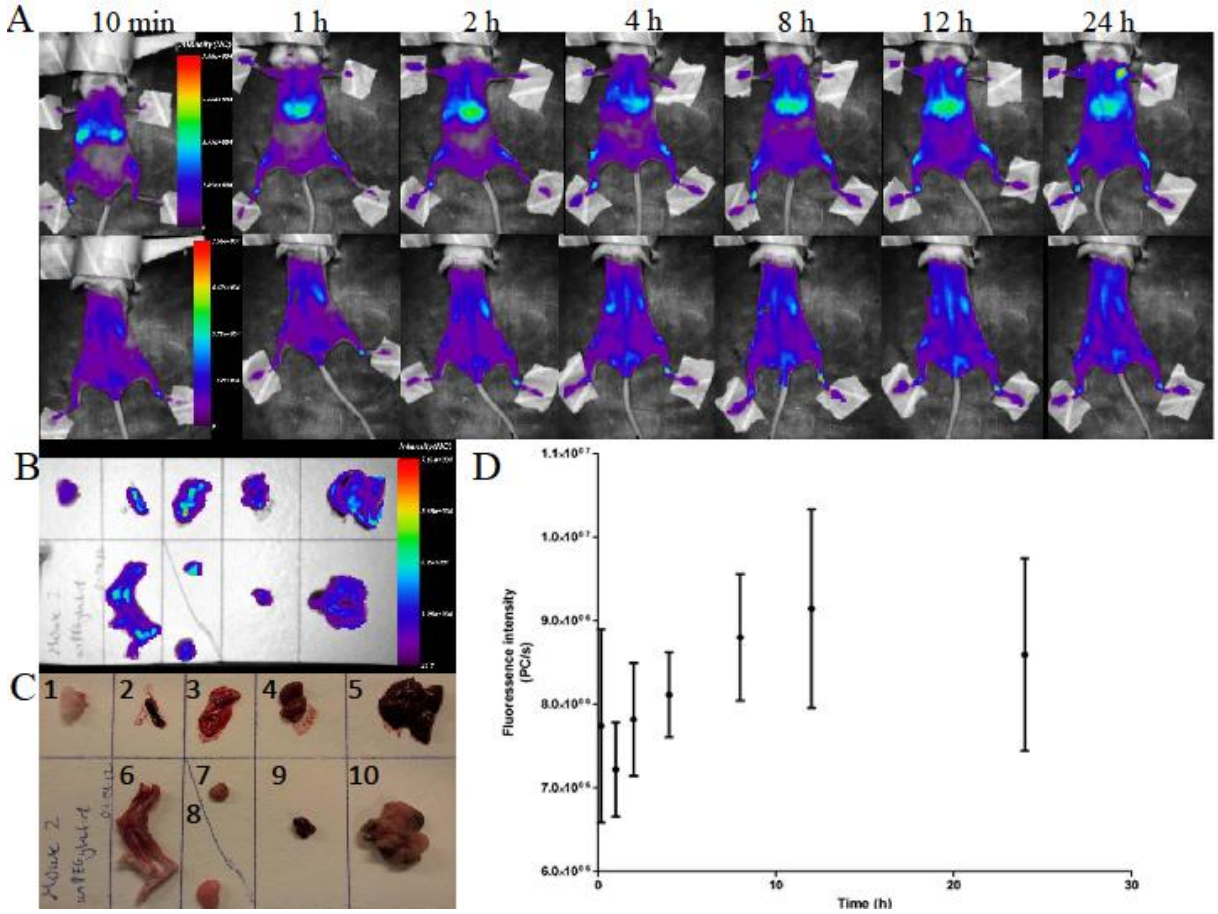

Figure 4.8 *Biodistribution of unPEGylated nanocapsules loaded with DiD. A: Development of fluorescence intensity (photon counts per second) at the different time points. Ventral and dorsal intensity is shown. B: Fluorescence intensity from the organs 24 hours post injection. C: Colour image of organs scanned.1: Skin, 2: Spleen, 3: Lungs, 4: Kidneys, 5: Liver, 6: Hind legs, 7: Brown adipose tissue, 8: White adipose tissue, 9: Heart,*

10: Intestine. D: Development of the fluorescence intensity over 24 hours. Ventral and dorsal maximum fluorescence is added at each time point (6 measurements).

A mouse was given free dye as a comparison to the encapsulated dye (Figure 4.9). The dye was dissolved in a small amount of pharmaceutical grade peanut oil, and emulsified by ultrasonication. An equivalent dose to the amount of dye in the nanocapsules was administrated through i.v. injection. The free dye showed high accumulation into the liver and some into the lungs. The free dye was also accumulated in the bones, clearly visible in the femurs and the spinal column (Figure 4.9 A). Fluorescence was seen in the adipose tissues, in addition to liver, spleen and some in the intestine (Figure 4.9 B and C). The fluorescence from the abdominal area was not as distinct as for the nanocapsules (Figure 4.7 and 4.8). The total fluorescence intensity (Figure 4.9 D) did not show the initial drop in fluorescence seen for the nanocapsules (Figure 4.7 D and 4.8 D). The animal injected with free dye show the lowest maximum fluorescence intensity ($0{,}428*10^7 \pm 0.52*10^6$ PC/s). This was measured after 12 hours.

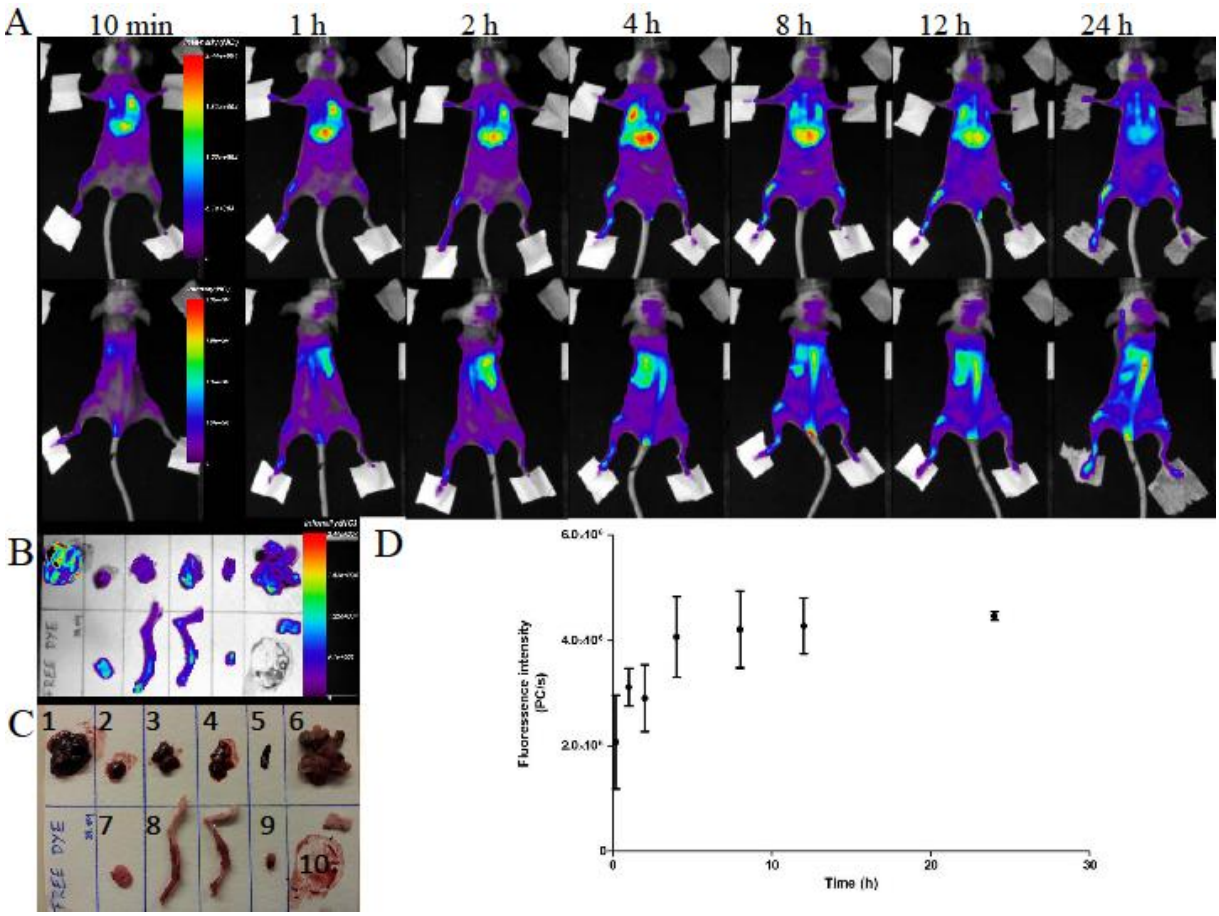

Figure 4.9 *Biodistribution of fluoresce from free dye. Panel A shows the development of fluorescence intensity (photon counts per second) at the different time points. Ventral and dorsal intensity is shown. B: The fluorescent*

intensity in the organs 24 hours post injection. C: Colour image of organs scanned. 1: Liver, 2: Heart, 3: Kidneys, 4: Lungs, 5: Spleen, 6: Intestine, 7: White adipose tissue, 8: Hind legs, 9: Brown adipose tissue, 10: Skin. D:Development of the fluorescence intensity over 24 hours. Ventral and dorsal maximum fluorescence is added at each time point (2 measurements).

The nanocapsules that were loaded with DiI instead of DiD showed similar biodistributions (Figure 4.13). The PEGylated nanocapsules (Figure 4.10 A) showed a stronger signal from the intestine than the unPEGylated nanocapsules (Figure 4.10 B) when loaded with DiI. This was similar to the nanocapsules loaded with DiD (Figure 4.7 and 4.8), and might indicate that PEGylated nanocapsules are more easily excreted into the intestine. The unPEGylated nanocapsules showed the strongest signals from the liver region. Due to technical problems with the eXplore optix imager, a laser with the wrong intensity was used to measure the nanocapsules loaded with DiI, and no quantification of the data was possible [20].

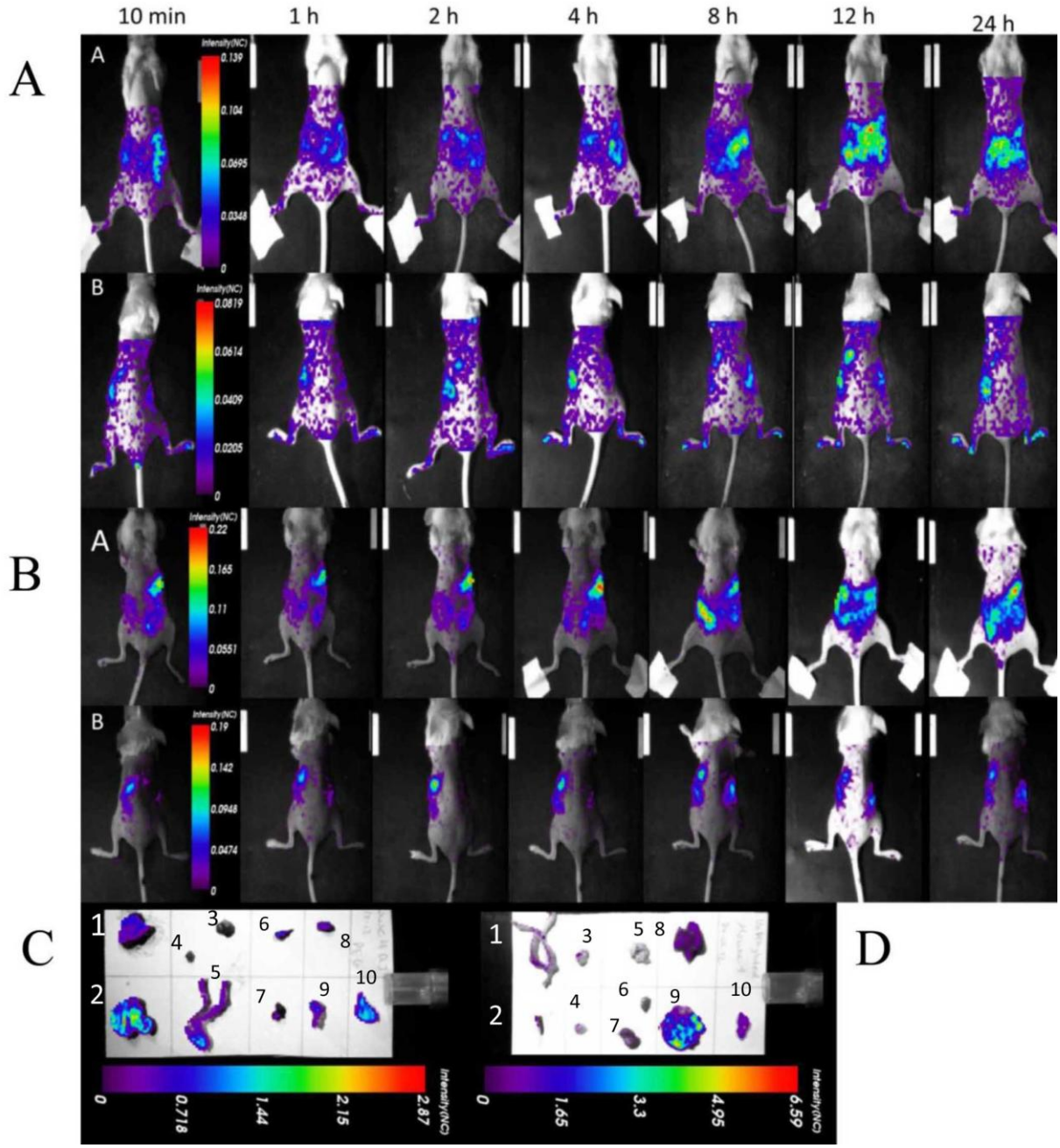

Figure 4.10 *Biodistribution of nanocapsules loaded with DiI. A: The development of fluorescence intensity (photon counts per second) at the different time points for PEGylated nanocapsules. Ventral and dorsal fluorescence is shown. B: The development of the fluorescence intensity for PEGylated nanocapsules. Ventral and dorsal fluorescence is shown. C: Fluorescence from organs 24 hours after injection with PEGylated nanocapsules; 1: Liver, 2: Intestine, 3: Lungs, 4: Brown adipose tissue, 5: Hind legs, 6: Spleen, 7: Kidneys, 8: Heart, 9: White adipose tissue, 10: Skin. D: Organ fluorescence from unPEGylated nanocapsules; 1: Hind legs, 2: Spleen, 3: Brown adipose tissue, 4: White adipose tissue, 5: Lungs, 6: Heart, 7: Kidneys, 8: Liver, 9: Intestine, 10: Skin.*

Analysis of the fluorescence lifetime was done to enable further interpretation of the biodistributions. Fluorophores change their lifetime according to the solvent they are dispersed in, and could give information about differences about whether the dye stayed encapsulated in or was released from the nanocapsules. A double exponential distribution with two lifetimes in different compartments was shown (Figure 4.11). One shorter lifetime was seen, which was measured mostly in the intestinal tract (Table 4.3), but that was different from the fluorescence lifetime of the autofluorescence. One longer lifetime was seen mostly in the liver, lungs and bone (Table 4.3). Estimations of the fluorescence lifetimes of the nanocapsules loaded with DiD in isotone solutions and free dye in a nanoemulsion of peanut oil were made in the imager system (Table 4.3). Also here two distinct lifetimes was seen for all solutions measured.

Table 4.3 *Fluorescence lifetimes of nanocapsules loaded with DiD; in solution (400 µL of nanocapsule solution measured) and in vivo (measurements made in the liver of three mice).*

Type of solution	Shorter fluorescent lifetime	Percentage of the short lifetime	Longer fluorescent lifetime	Percentage of the long lifetime
PEGylated nanocapsules in solution	0.60	78.5	1.76	21.5
unPEGylated nanocapsules in solution	0.44	77.2	1.68	22.8
Free dye in solution	0.37	66.7	1.24	33.3
PEGylated nanocapsules in vivo	0.41 ± 0.004	74.5 ± 1.50	1.55 ± 0.02	25.5 ± 1.49
unPEGylated nanocapsules in vivo	0.34 ± 0.02	72.0 ± 0,70	1.33 ± 0.05	28.0 ± 0,69

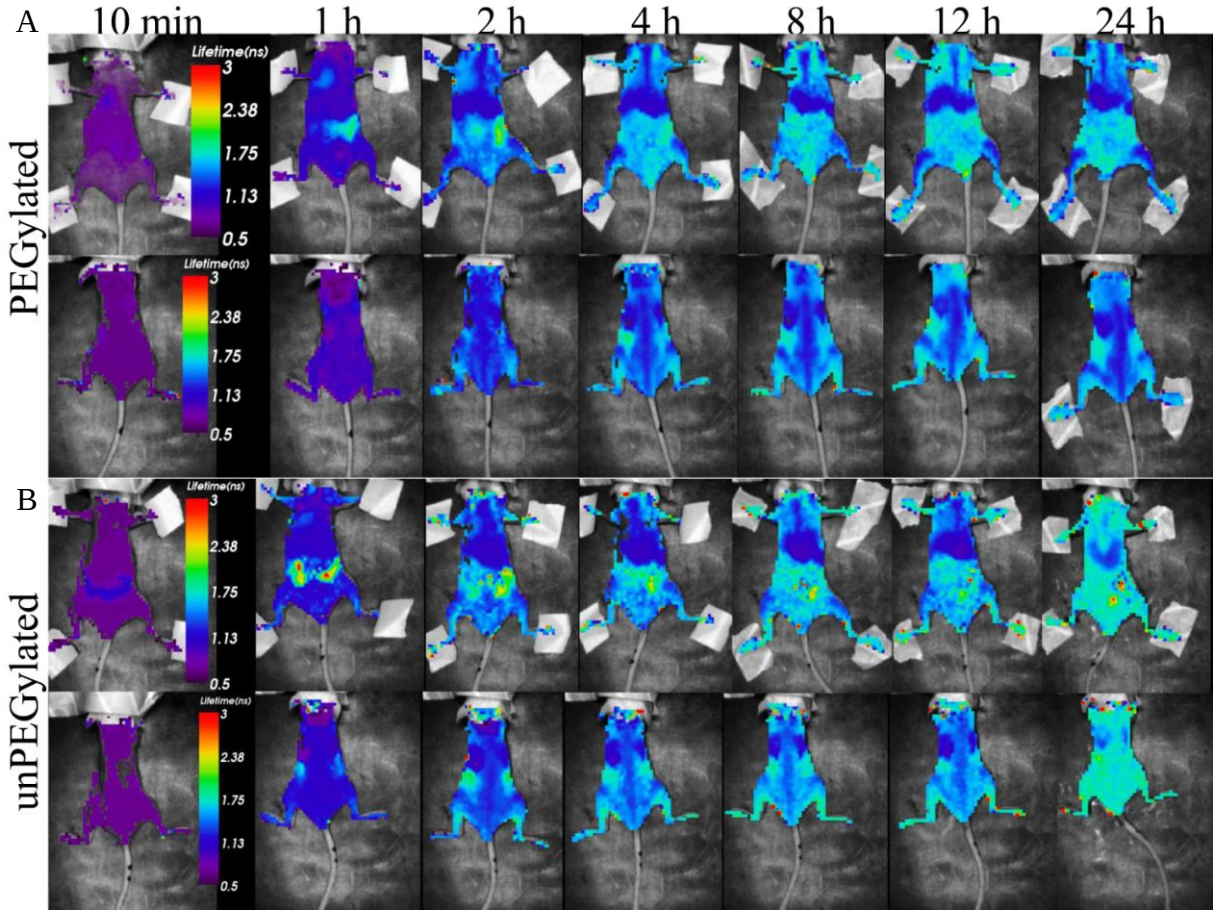

Figure 4.11 *Fluorescence lifetime of PEGylated (A) and unPEGylated (B) nanocapsules loaded with DiD over 24 hours. Fluorescence lifetime of both ventral and dorsal pixels is shown.*

The lifetime was portrayed as fluorescence lifetime histograms (Figure 4.12 A and B). These showed a shift from the shorter fluorescence lifetime (around 0.8 ns) to the longer fluorescence lifetime (around 1.2 ns). Both types of nanocapsules showed clear dominance of the shortest lifetime after 10 minutes, this is most evident for the PEGylated nanocapsules (Figure 4.12 A). The unPEGylated nanocapsules had a more divided distribution between the lifetimes from the start (Figure 4.12 B). Over the next hours a more divided distribution of the two lifetimes were seen, probably indicating accumulation in different tissues and/or transfer to lipoproteins. After 24 hours the longer fluorescence lifetime predominates, both for the PEGylated and unPEGylated nanocapsules. Lifetimes were recorded from pixels in the liver of three mice, and the average percentage of the two lifetimes over the 24 hours (Figure 4.12 C and D).

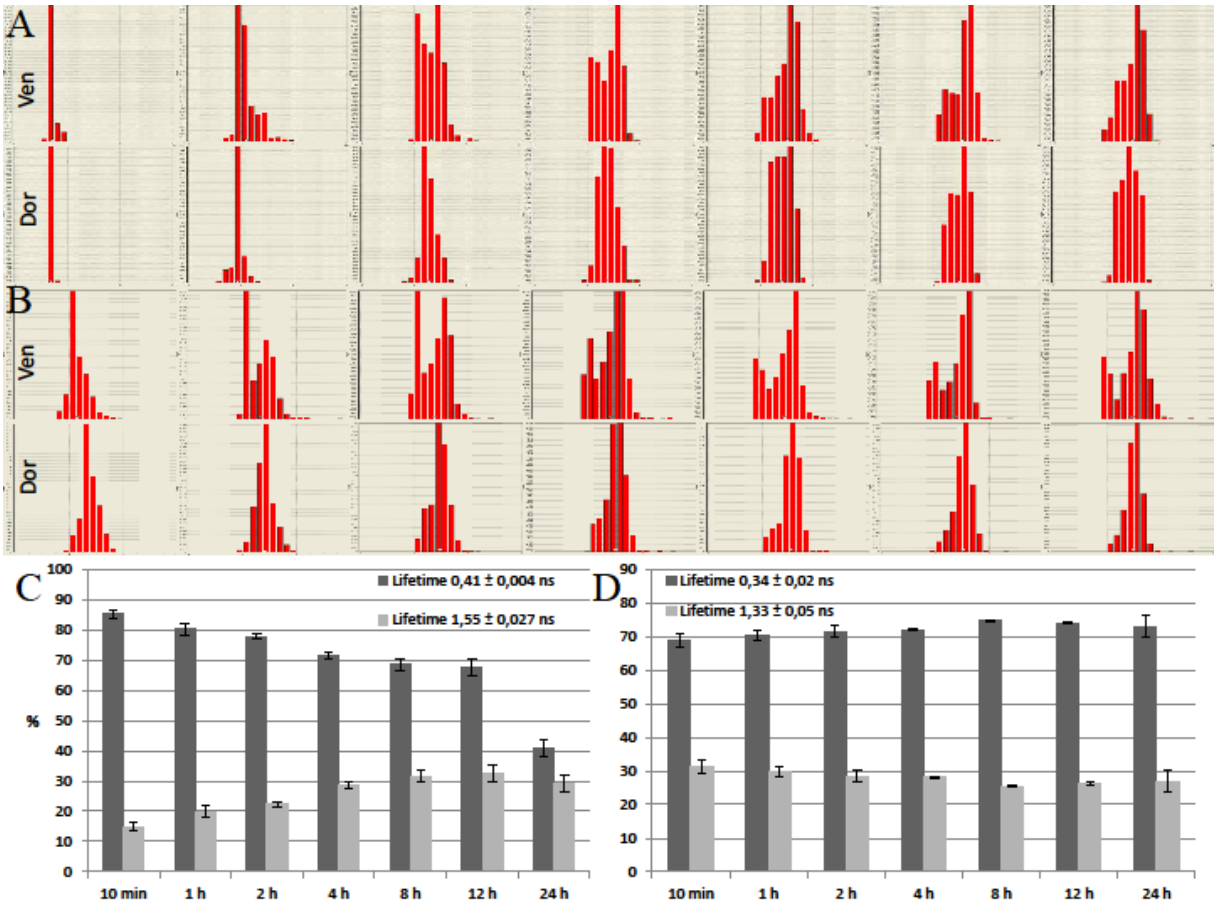

Figure 4.12 *Panel A and B shows fluorescence lifetime histograms for PEGylated and unPEGylated nanocapsules, respectively. Both ventral and dorsal fluorescence is shown. The x-axis show fluorescence lifetime in nanoseconds (0-3) and the y-axis represent intensity. C and D: Percentages of the two fluorescent lifetimes from pixels in the liver for PEGylated nanocapsules (C) and unPEGylated nanocapsules (D). The PEGylated nanocapsules showed a distinct shift over the 24 hours. The unPEGylated nanocapsules show no such shift.*

These showed that the PEGylated nanocapsules (Figure 4.12 C) had a distinctive transition from the shorter fluorescence lifetime towards the longer lifetime. The unPEGylated nanocapsules (Figure 4.12 D) show no such shift in the fluorescence lifetime over the 24 hours; however a minor shift in the opposite direction towards the longer fluorescence lifetime was detected.

4.2.2 Biodistribution of solid nanoparticles labelled with Texas red (DY-700)

Next we wanted to find out if the time related changes in tissue distribution of fluorescence incorporated in nanocapsules reflected nanocapsule localization, or if fluorescent dye had leaked from the capsules. We wanted to look for differences in biodistribution of the solid nanoparticles and the nanocapsules. As rhodamine has excitation and emission below the NIR window, it cannot be used in the imaging systems and we decided used PLGA polymer covalently linked to Texas red dye DY-700 for this. The biodistribution of particles conjugated to DY-700 was investigated by NIR imaging with X-ray since the dye-loaded nanocapsules showed strong fluorescence from the areas around the femurs, sternum and spinal column (Section 4.2.3).

The fluorescence scans of the animals injected with PEGylated nanoparticles showed generalised fluorescence that was hard to distinguish from the background fluorescence (Figure 4.13). This was probably due to technical problems during the scans. However, we noted strong fluorescence from the intestine, spleen and white adipose tissue. Fluorescence was also seen from the kidneys (Figure 4.13 B and C). Less was seen in the liver and lungs. Fluorescence from the bones was not seen. The development of maximum fluorescence intensity over 24 hours is shown (Figure 4.13 D). The intensity was the highest after 10 minutes and gradually declines until 8 hours. The intensity then increased.

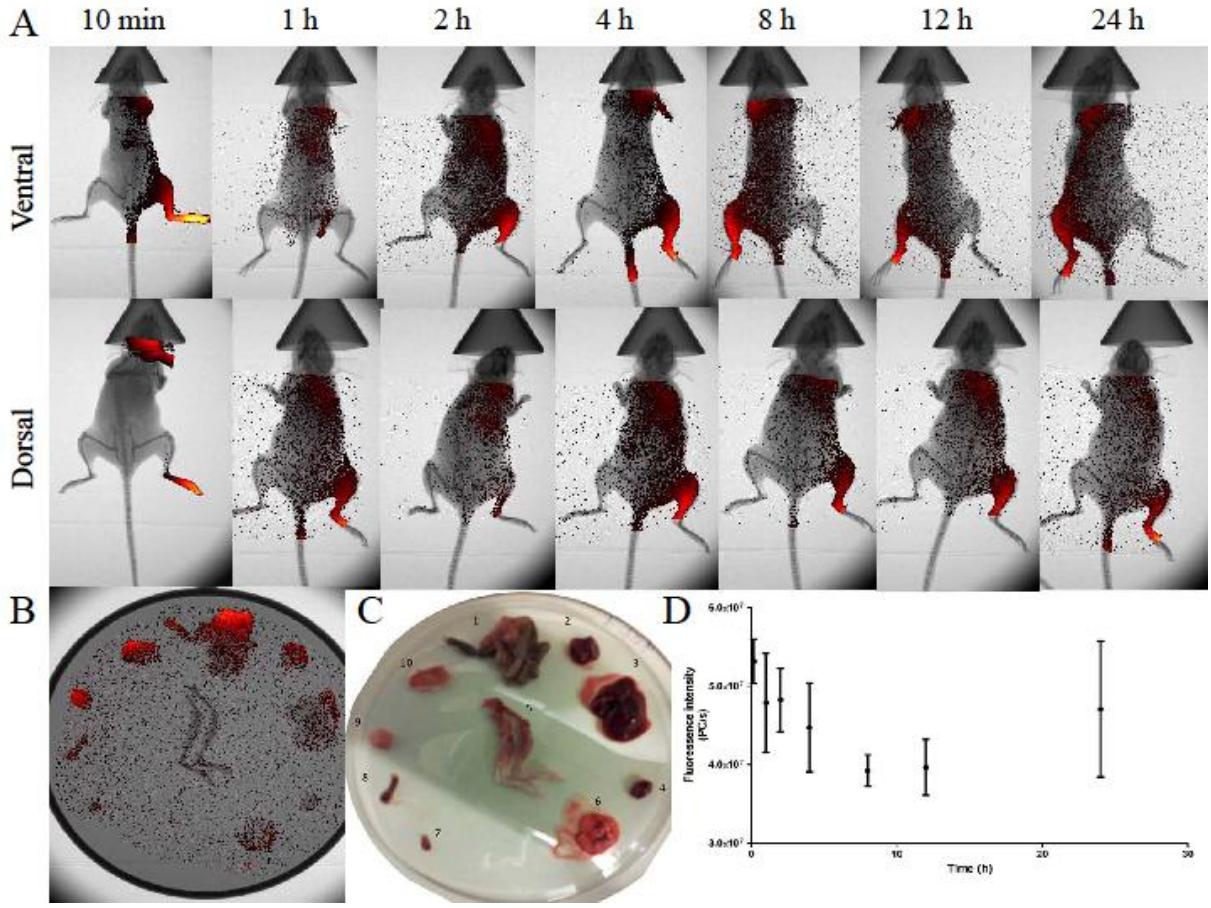

Figure 4.13 *Biodistribution of PEGylated nanoparticles conjugated to a Texas red dye. A: Development of fluorescence intensity (photon counts per second) at the different time points. Ventral and dorsal intensity is shown. B: Fluorescence intensity in the organs after 24 hours. C: Colour image of organs scanned. 1; Intestine, 2; Kidneys, 3; Liver, 4; Heart, 5; Hind legs, 6; Lungs, 7; Brown adipose tissue, 8; Spleen, 9; White adipose tissue, 10; Skin. D: Development of total fluorescence intensity over 24 hours. Ventral and dorsal maximum fluorescence is added at each time point (2 measurements).*

The mice injected with unPEGylated solid nanoparticles conjugated to DY-700 showed a similar biodistribution over the 24 hours as the mice injected with PEGylated nanoparticles. The development of the fluorescence intensity over 24 hours is showed in Figure 4.14 A. The intensity was the strongest after one hour ($1.42*10^8 \pm 3.245*10^7$) and then declined towards 24 hours (Figure 4.14 D). At ten minutes most of the fluorescence was in the abdomen and lungs. The fluorescence intensity was then mainly seen in the liver and the abdomen. In contrast to the PEGylated solid nanoparticles, we found that the unPEGylated solid nanoparticles, most of the fluorescence was found in the liver after 24 hours. The organs scans reflected these findings (Figure 4.14 B and D), and fluorescence was mainly seen from liver and spleen, with some signal from the intestine and the lungs. The unPEGylated nanoparticles

showed stronger accumulation in the liver than the PEGylated particles showed, but less in the intestine. The PEGylated nanoparticles also showed a signal from the adipose tissues. No such signal was seen for the unPEGylated nanoparticles. UnPEGylated nanocapsules (Figure 4.8) showed a large signal from the lungs, this is not seen when the dye is covalently bound. In addition there were seen differences between the amounts in femurs, and the adipose tissues.

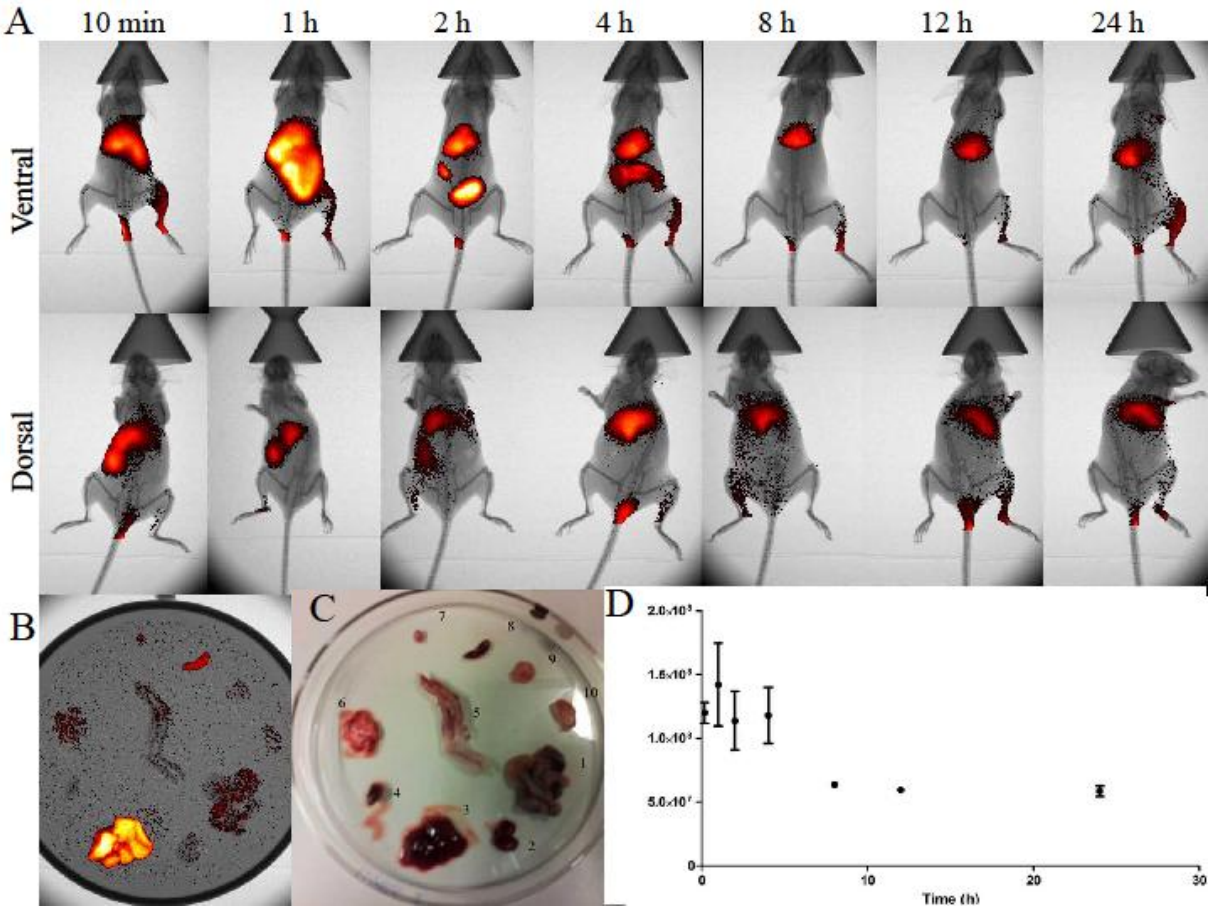

Figure 4.14 *Biodistribution of unPEGylated nanoparticles conjugated to a Texas red dye. Panel A shows the development of fluorescence intensity (photon counts per second) at the different time points. Ventral and dorsal intensity is shown. Panel B shows the fluorescence intensity in the organs after 24 hours. Panel C; Colour image of organs scanned. 1; Intestine, 2; Kidneys, 3; Liver, 4; Heart, 5; Hind legs, 6; Lungs, 7; Brown adipose tissue, 8; Spleen, 9; White adipose tissue, 10; Skin. Panel D shows the development of the fluorescence intensity over 24 hours. Ventral and dorsal maximum fluorescence is added at each time point (2 measurements).*

4.3 Ex vivo analysis of fluorescence accumulation

4.3.1 Microscopic analysis of tissue and organ distribution of solid nanoparticles labelled with rhodamine

To find out more about the tissue distributions of fluorescently labelled nanocolloids, we injected i.v. with solid nanoparticles with rhodamine covalently linked to the polymer backbone. After 24 hours the mouse was sacrificed, and tissue removed for examination by confocal microscopy. The positive cell counts show a preference for tissues such as liver, spleen and lungs (Figure 4.15). This is also visible as high amounts of positive cells in these tissues on confocal microscopy investigations (Figure 4.16 A-F and J-L). A high amount of the carriers were also found in brown adipose tissue (Figure 4.15 and 4.16 G-I). In the lungs (Figure 4.16 J-L) and skin (Figure 4.16 M-O) some nanoparticles were seen, and few or none carriers were seen in the kidneys, the heart and white adipose tissue (Figure 4.15).

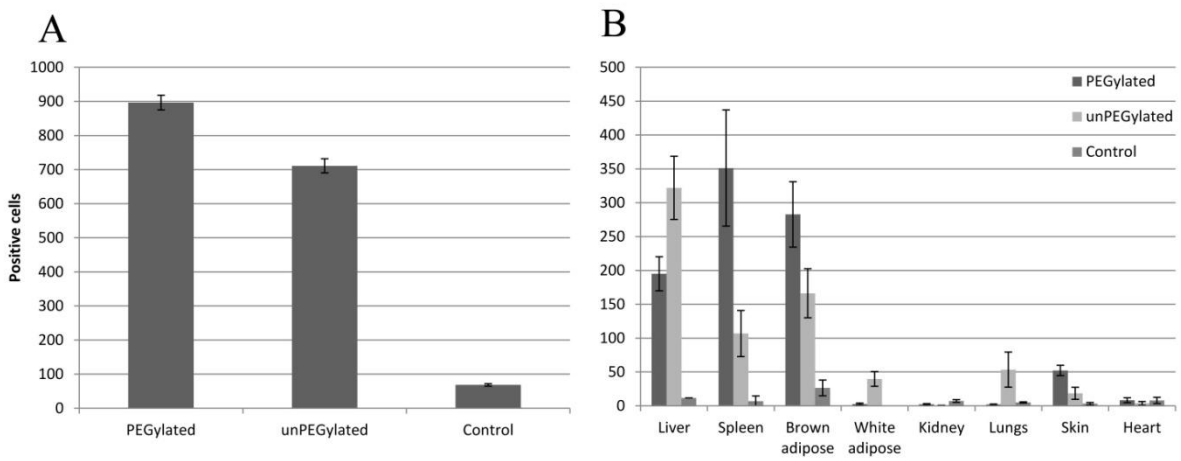

Figure 4.15 *A: Total counts for the different parallels. B: Estimations of positive cells in the different tissues 24 hours after injection of solid nanoparticles covalently labelled with rhodamine. All counts are given as the mean of 4 measurements. PEGylated particles, unPEGylated particles and a control (not given nanocolloid) are shown.*

The counts of total positive cells in the tissues showed a lager quantity of PEGylated than unPEGylated particles in the tissues. This could indicate that the PEGylated nanoparticles are present to a higher degree after 24 hours, and a higher portion of the unPEGylated nanoparticles might be degraded at this point. The largest differences were seen in the tissues with the highest counts (Figure 4.15). The unPEGylated tissues show larger accumulation in the spleen (Figure 4.16 D-F), brown adipose tissue (Figure 4.16 G-I) and skin (Figure 4.16 M-O) than the PEGylated nanoparticles. The PEGylated nanoparticles showed larger accumulation in the liver (Figure 4.16 J-K), white adipose tissue and the lungs (Figure 4.16 J-K) than does the unPEGylated nanoparticles. The larger accumulation in the liver and lungs suggests that particles that have been taken up by macrophages present in these organs. Notice that the unPEGylated are mainly accumulated in the liver, while the PEGylated are mainly in the spleen and brown adipose tissue.

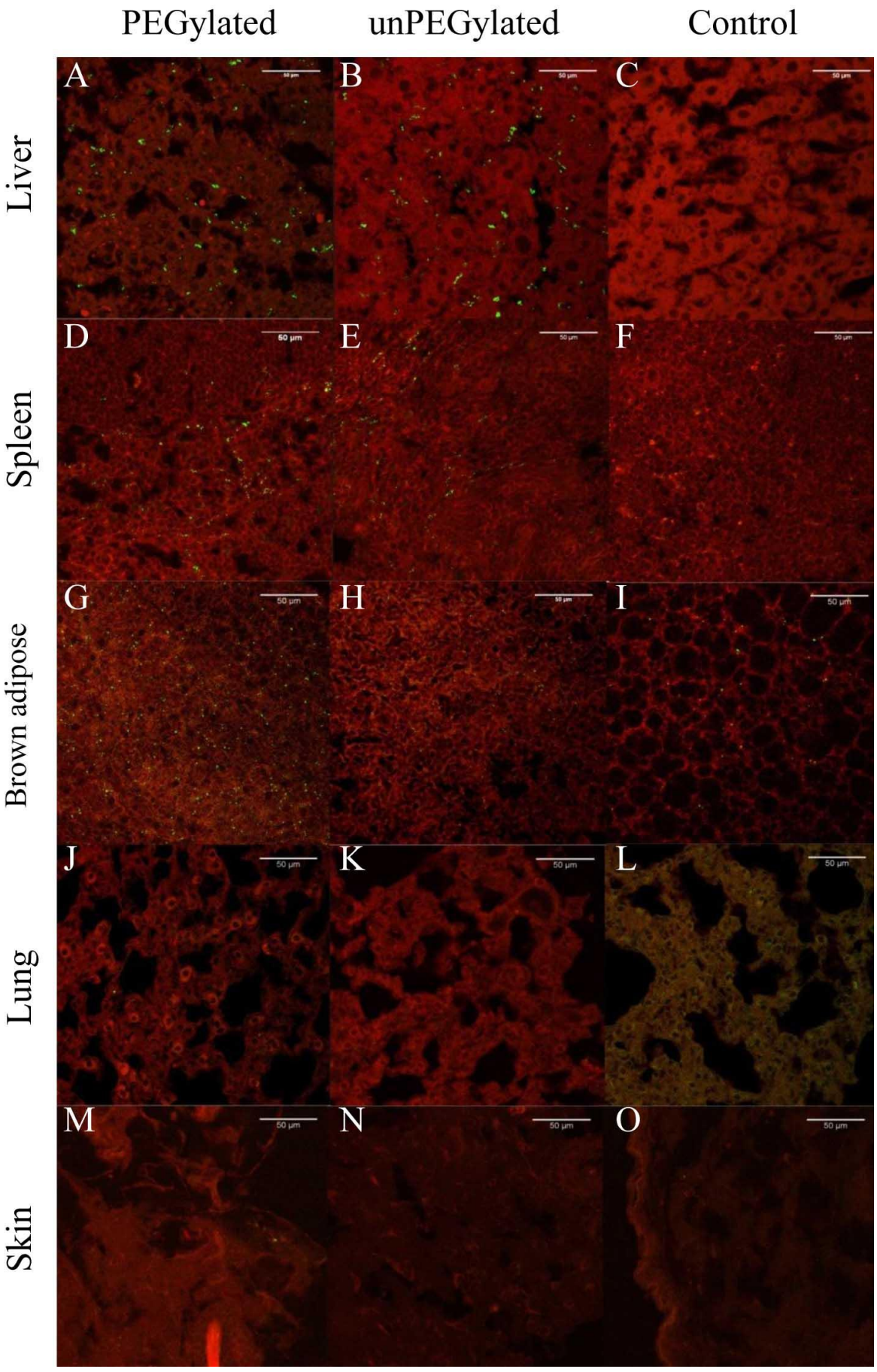
PEGylated
unPEGylated
Control
Liver
Spleen
Brown adipose
Lung
Skin
A
B
C
D
E
F
G
H
I
J
K
L
M
N
O
50 µm

Figure 4.16: *Presentation of fluorescence in tissues when mice were injected with nanoparticles conjugated to rhodamine. The greatest amounts of positive cells were seen in the liver (A-C), spleen (D-E) and brown adipose tissue (G-I). Some positive cells where seen in the lung (J-L) and skin (M-O). Note that rhodamine is portrayed as green (dots), while background fluorescence is portrayed as red.*

4.3.2 Fluorescence accumulation in bone marrow.

It was noted that fluorescence seemed to accumulate in the bone or bone marrow of the mice injected with nanocapsules with or without PEG (Figure 4.7-4.11). Bone marrow was therefore collected and investigated for fluorescent content. Bone marrow was also collected from a mouse that did not receive nanocolloid injection to function as a negative control. This sample had fluorescence intensity of -0.18 ± 0.02, and we concluded that no autofluorescence was present in the bone marrow at the wavelength used.

The strongest fluorescence were measured from the bone marrow of the mice injected with nanocapsules loaded with DiD (figure 4.17 A). This was also seen in the images for the NIR imaging (Figure 4.7-4.11). The PEGylated had about five times higher fluorescence intensity in their bone marrow (Figure 4.17 A). The nanocapsules loaded with DiI showed the same trend (Figure 4.16 B) with a high degree of fluorescence from the PEGylated capsules and less from the unPEGylated capsules. Note that the nanocapsules loaded with DiI contained less dye (0.174 µmoles) than the nanocapsules loaded with DiD (0.275 µmoles). T test were only preformed if more than three parallels were available.

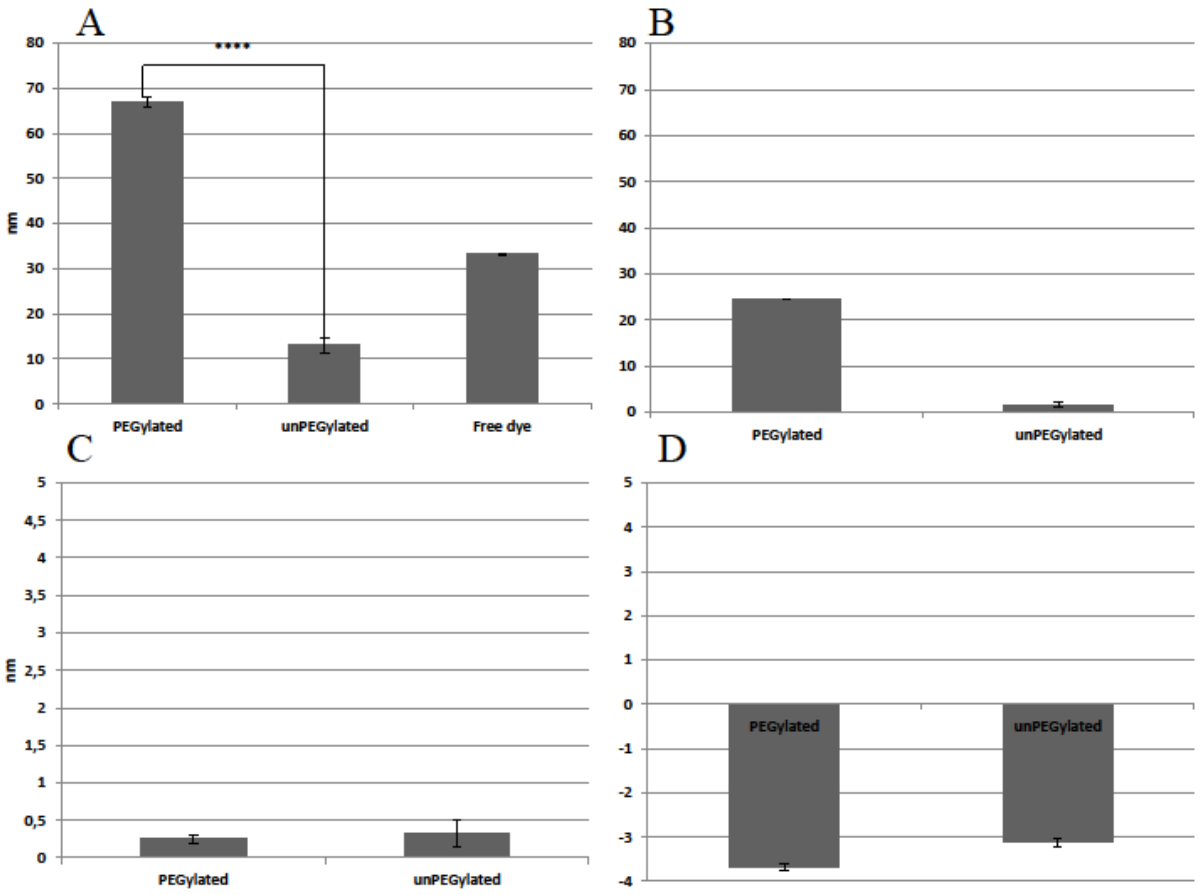

Figure 4.17 *Measurements of fluorescence in bone marrow. A: Mice injected with DiD loaded nanocapsules. B: Mice injected with nanocapsules loaded with DiI. C: Mice were injected with nanoparticles conjugated to DY-700. D: Mice were injected with nanoparticles conjugated to Rhodamine. Note the differences in scale in Y-axis in A to D. T test were performed when there were more than three parallels were available (A, C).*

None of the mice injected with either type of solid nanoparticles showed any accumulation of fluorescence in the bone marrow (Figure 4.17 C and D). The mice injected with solid nanoparticles conjugated to DY-700 showed florescence close to zero both for the PEGylated and unPEGylated kind. T-test showed no significant difference between the two groups (P-value: 0.74). The mice injected with solid nanoparticles conjugated to Rhodamine showed negative measurements of fluorescence, both for the PEGylated and unPEGylated kind. It was concluded that fluorescence does not travel to the bone marrow when conjugated to the polymer.

5 Discussion

5.1 Evaluation of nanocolloids produced.

The safe delivery of therapeutically active ingredients to their desired site of action without unwanted effects on other tissues is challenging to achieve. We have used nanoprecipitation (Figure 4.1), a well established and easily up-scalable method [22, 23], for the production of PLGA nanocolloids for use as drug delivery systems and NIR fluorescent contras agents (Figure 1.5 and 1.6). The nanocolloids produced have the opportunity to be used as theranostics. The method uses a safe and biocompatible polymer, PLGA, which is approved by the FDA. A biocompatible stabiliser was used only when necessary, and non-chlorinated solvents were used. Chlorinated solvents are toxic, and could degrade some drugs and proteins [4]. All the ingredients are already used in the pharmaceutical industry, and are of low cost. The process requires little input of energy, as no ultrasonication or other high energy requiring methods were used. This means lower production costs on large scale. The nanocolloids biodistributions were traced *in vivo* through NIR optical imaging and the results were evaluated together with *ex vivo* examinations of organs and tissues.

The drug delivery systems were produced with the delivery of chemotherapeutics in mind. Chemotherapeutics often have a low aqueous solubility and high toxicity [37]. The latter is necessary to eliminate the cancer cells, but can also lead to severe side effects on healthy tissues. Incorporation of the drugs in nanocolloids means that the use of drugs with low aqueous solubility can be more easily achieved, without chemically changing the drug, and the exposure of the chemotherapeutic to healthy tissues is significantly decreased [27, 30]. It is hoped that the nanocolloids produced in the presented study is designed to function in a similar manner and it is therefore necessary with careful *in vivo* examinations of the nanocolloids distributions and pharmacokinetic patterns.

All the nanocolloids produced were of a size that allows for intravenous injection, normally recognized as below 5 µm [40]. A capillary is around 8 µm [41]. The size distributions were monodisperse (Figure 4.1-2 and 4.4) and the oily core nanocapsules (Table 4.1 and Figure 4.3) were bigger than the solid nanoparticles (Table 4.2). The size of the nanocapsules is influenced by the size of the oily core. All nanocolloids had low polydispersity indexes (Table 4.1 and 4.3) and low batch to batch variations were seen. The oily core nanocapsules showed slightly higher polydispersity indexes than the solid nanoparticles (Table 4.1 and 4.2), which

is in line with other studies on this type of nanocolloid [42]. The same study showed a strong influence of lecithin on the zeta potentials of nanocolloids, and concluded that high concentrations of soy lecithin imparted a low negative zeta potential at around –45 mV. This is not in concurrence with the results obtained here, where the solid nanocolloids showed the lowest zeta potential (Table 4.1) and the nanocapsules showed markedly higher zeta potentials (Table 4.2). Another study showed zeta potentials closer to neutral [20], and the zeta potentials measured here were between these two results. It might be that differences in the methods used for producing the nanocolloids influences how the polymers and lipids orient themselves and therefore also characteristics such as zeta potential. Another possible explanation is that different dispersion mediums were used for the measurements, namely 5 % glucose (the present study), PBS [20] and 9 mg/ml NaCl [42]. The zeta potential is highly influenced by pH and ionic concentrations.

The nanocapsules with an oily core were shown to be stable for up to one month in water (Figure 4.5), probably due to steric stabilisation from the PEG chains present (Figure 1.4). Other has shown good stability of these nanocolloids [19]. The different stabilisers tested for use with the solid nanoparticles (Figure 4.3) did not seem to influence the nanoprecipitation itself, but had an effect during washing. This shows that the type of stabiliser can be varied to fit the type of PLGA polymer and drug chosen to produce the nanocolloids. The use of stabiliser is in itself somewhat problematic, as residues of the molecule can stay dissolved in the nanocolloid solution or associate/adsorb on the polymer matrix and this have been showed to affect the properties of the nanocolloids [2]. Less is known about the effect of residual stabiliser on nanocolloids distribution, release and degradation. But it is known that the type of drug incorporated in nanocolloids can influence the properties of the polymer [11], and it is therefore likely that residual stabiliser will do the same. Here we decided to use low concentrations of sodium cholate as stabiliser. This is biocompatible, with minimal side effects compared to for instance PVA and related detergents [43]. We were also able to demonstrate the possibility of production of oily core nanocapsules without the use of a stabiliser. These are generally made with stabilisers such as poloxamer 188 [30, 32], but evidence of stabilisation by entrapped lipids in the oily core should indicate that these nanocolloids could to be produced without the aid of a stabiliser [19, 20]. When nanocolloids where washed with PBS, they had a tendency to flocculate, probably due changes in the ionic strength of the dispersion medium. Isotonic sucrose was used instead, and have also been used in other studies [30]. The nanocapsules produced without stabiliser showed an increase of

polydispersity index after addition of glucose. The nanocapsules also showed a marked increase in size after incubation with BSA (Figure 4.6). The solid nanoparticles showed none of these characteristics. This might indicate that the nanocapsules made without stabiliser are more easily affected by changes in the dispersion medium than the solid nanoparticles. The incorporation of the fluorescent dyes into the PLGA polymer has been shown to not affect the size, morphology and PDIs of the nanocolloids produced [20, 36]. The incorporation should also not negatively affect the fluorescent properties of the dyes incorporated [28].

5.2 Comparison of the biodistributions of PEGylated and unPEGylated nanocolloids:

The nanocapsules with an oily core appeared to accumulate mainly in the intestinal track, liver, lungs and bone (Figure 4.7 and 4.8). Both the PEGylated and the unPEGylated nanocapsules showed this pattern, but the development was different over time. The PEGylated nanoparticles (Figure 4.7) showed the strongest signal from the liver and lungs up to four hours, and after this an increase in fluorescence from the bones and the general lower abdomen was seen. There was also an accumulation of fluorescence in the upper neck (Figure 4.7 dorsal pictures), an area known to contain brown adipose tissue [44], visible already after 10 minutes, and further accumulation over the 24 hours are detected. The fluorescence intensities (Figure 4.7 D) showed a drop from ten minutes to one hour. This is probably due to distribution of fluorescence in the tissues. The fluorescence intensity then rises again until 12 hours, where it seems to reach a plateau.

The unPEGylated particles (Figure 4.8) showed a distinct and increasing uptake into the liver and spleen over the 24 hours, which was not seen to this extent for the PEGylated nanocapsules. This might indicate more circulating PEGylated particles and more accumulation of the unPEGylated particles in the liver over the 24 hours. A distinct and slowly accumulating fluorescence from the femurs was also visible for the unPEGylated nanocapsules. Less accumulation of fluorescence was seen from the lower abdomen, and the dorsal fluorescence in the area rich in brown adipose tissue developed only after 8 hours. The fluorescence intensities (Figure 4.8 D) shows the same drop in signal from 10 minutes to 1 hour, but it is not as marked as for the PEGylated nanocapsules. The signals start to decrease after 12 hours, not seeming to reach the plateau seen for the PEGylated nanocapsules. This might indicate less capture of the PEGylated nanocapsules by macrophages.

The free dye (Figure 4.9) showed clear signals from the lungs and liver, and in the liver the intensity start to decrease after 8 hours, indicating metabolism of the dye. An interesting observation was that the bone marrow appeared to have the highest fluorescence intensity. The accumulation in the spine is particularly visible on the dorsal images, peaking at 24 hours. It might be that the uptakes of fluorescence into bone seen for the nanocapsules are of free dye either from the surface of the particles or dye that has escaped the nanocapsules, and not the nanocapsules themselves.

As expected, the type of fluorophore did not affect the distribution of fluorescence. The mice injected with DiI (Figure 4.13) showed similar biodistributions to the nanocapsules loaded with DiD. The PEGylated nanocapsules (Figure 4.13 A) showed accumulation in the liver and maybe lungs the first hours, and after 4 hours an increase in the intestine is seen towards the 24 hours. Accumulation in the intestine and spleen was seen for the unPEGylated nanocapsules (Figure 4.13 B), maybe an indication of more metabolism of these nanocolloids. Interestingly there are reports that the more blue-shifted DiI do not produce an signal in the NIR window [20]. However, in our system, DiI produced clear signals, but due to a defect in the laser intensity adjustment, the power used was too low to record data with sufficient fluorescent intensities.

The unPEGylated solid nanoparticles labelled with DY-700, had mostly accumulated in regions corresponding to the liver 10 minutes after injection (Figure 4.14). After one hour the whole lower abdomen showed strong fluorescence. The fluorescence then relocated towards the liver and spleen over the 24 hours. The organ showed fluorescence from the lungs for the PEGylated nanoparticles (Figure 4.13) but not for the unPEGylated, which differs from the results seen ex vivo, where the unPEGylated nanoparticles showed accumulation in the lungs (Figure 4.15). The organs also showed a high amount of fluorescence in the intestine for the PEGylated, but less for the unPEGylated nanoparticles. This could indicate that more of the PEGylated nanocapsules remain in the circulation after 24 hours. The intensity of total fluorescence (Figures 4.13-14 D) was highest for the PEGylated nanoparticles. The curve decreased towards 8 hours and then starts to increase again. One possibility is that the dye has started to be released from the polymer at this point. The unPEGylated nanoparticles had a lower maximum intensity and it is seems to be stabilising after 24 hours. This also indicates a higher elimination of the unPEGylated than the PEGylated nanoparticles after 24 hours. Unfortunately, due to technical problems the mice injected PEGylated nanocapsules gave

poor intensity reading on the *in vivo* scans and to further compare unPEGylated and PEGylated solid nanoparticles further investigations are needed.

Taken together, the unPEGylated nanocolloids produced are more quickly accumulated in the liver. The PEGylated nanocolloids appear to have a longer circulation time. The oily core nanocolloids showed increasing amounts in the intestine, seen after 8 hours for the unPEGylated nanocapsules, and 12 hours for the PEGylated nanocapsules. The PEGylated nanocapsules also seem to have more stable fluorescence intensity after the 24 hours. The solid nanoparticles show less accumulation in the intestine, and were mostly accumulated in the liver after 24 hours. Both types the nanocapsules and the solid nanoparticles showed a stronger over all fluorescence from the PEGylated nanocolloids. This is also indicative of a faster removal from the blood stream of the unPEGylated nanocapsules.

The fluorescence lifetime of the nanocapsules were investigated to further understand the fluorescence biodistributions. These analyses showed that there were two distinct lifetimes present both in the nanocapsules, in free dye (in peanut oil), and in the animals (Table 4.3). There was a shift from the shorter lifetime towards the longer lifetime as time progressed (Figure 4.12) indicating a change of state of the dye, such as accumulation in constituents in the blood, for instance plasma proteins or lipoproteins, and in other tissues. The shorter lifetime seems to accumulate in the intestinal tract (Figure 4.11), both for PEGylated and unPEGylated nanocapsules, also visible in the organs after 24 hours (Figure 4.7-8 and 4.14-15). The longer lifetime was mostly seen in the liver, spleen and bone marrow, tissues rich in macrophages. Interestingly, there was a transition of lifetime from shorter to longer in the liver in animals injected with PEGylated nanocapsules (Figure 4.12 C), but not in animals injected with unPEGylated nanocapsules (Figure 4.12 D). This can indicate leakage of dye from PEGylated nanocapsules taken up by e.g. macrophages. If seen together with the results from the fluorescence intensity investigations this gives a strong indication that the nanocolloids or the fluorophore itself are transported to the lymphatic circulation after capture by macrophages, and drained out into the intestine [20, 32]. Also the solid nanoparticles were accumulated the liver and spleen (Figure 4.15) and taken together this indicates that nanocolloids are accumulated organs such as the liver and spleen (Figure 4.16), while the free dye is accumulated in bone marrow, as indicated when fluorescence was measured in bone marrow collected (Figure 4.17). Indications of metabolism of this free dye were seen in the liver (Figure 4.9), but an interesting question raised is how long the dye taken up into bone will remain before metabolism occurs. DiD loaded nanocapsules have shown signals from the

liver for up to a few weeks [20], and further investigations around the properties of the dyes *in vivo* are needed. The solid nanoparticles showed no fluorescence from the bones (Figures 4.13, 4.14 and 4.17), which points toward only free dye being incorporated into the bone marrow, and not the nanocolloids themselves.

The effect of PEGylation was also investigated inside tissues *ex vivo* through confocal microscopy (Figure 4.15 and 4.16), as no precise calculations can be done though NIR *in vivo* imaging. These results were similar to the distributions seen in vivo, and the PEGylated nanoparticles were found in the greatest amount (Figure 4.16). The high counts were due to the large accumulation in the spleen and brown adipose tissue that was not seen for the unPEGylated nanoparticles. It was found a higher count of the unPEGylated nanoparticles in the liver and the lung, similar to what has been found in other studies [45]. This is likely to be particles captured by macrophages. The accumulation in the lungs was not visible during in vivo imaging. The Fluorescence might be situated too deep to be effectively transmitted *in vivo*. The large accumulations in the spleen for the PEGylated nanocolloids might not be visible for the same reason. A large accumulation in brown adipose tissue was seen for both kinds of particles, the largest accumulation for the PEGylated nanocapsules. This is interesting, as it gives an indication of the effect of both the EPR theory and the effect of PEGylation; Brown adipose tissue has fenestrated capillaries [44], and the nanocolloids produces do show retention in the tissue. In addition the PEGylated were present in the largest amount (Figure 4.15). This indicates that they circulated longer, so that a larger amount could reach the brown adipose tissue. This gives an indication that the nanocolloids produced here could be used as drug delivery systems that passively target tumours, as they also have fenestrated capillaries [12]. Passive targeting using similar nanocolloids have been demonstrated in several tumour models [27, 37]. PEGylation of PLGA has been shown to lead to longer circulation times as it prevents opsonisation and capture by macrophages. PEG chains over 20 kDa have shown the best results at preventing uptake in macrophages *in vitro* [42], another study showed that the nanocolloids with a high PEG content had more degradation over 7 days at 37 °C [45]. This further shows the need for *in vivo* studies of each specific drug delivery system envisioned [26].

5.3 Differences in biodistribution when the fluorescent dye is loaded or covalently bound to the polymer.

One challenge when using nanocolloids for *in vivo* optical imaging is that we cannot visualise the nanocolloids themselves, only record the fluorescence. Particularly with the nanocapsules with an oily core this could be problem, and significant leakage of the fluorescent dyes during circulation has been reported [6]. There could also be a small amount of dye dissolved in the aqueous phase of the suspension which complicates the data analysis further. To avoid this problem, the nanocapsules could be dialysed or gel filtrated [20, 37]. Leakage of DiD during storage have been seen for similar nanocapsules [20]. Oily core nanocapsules have been shown to have encapsulation efficacy above 90 % for the carbocyanine dyes, including DiD and DiI, and the loading of the dye had no influence on the diameter, size distribution or zeta potentials [20].

The use of nanocolloids produced with fluorescent dyes covalently linked to the polymer should experience no leakage, as the dyes covalent bonds to the polymer backbone have to be broken before any free dye can be seen *in vivo.* PLGA polymers with a ratio of PLA:PGA of 50:50 like the one used here have demonstrated the fastest degradation rates [11, 26]. Half lives of PLGA nanocolloids are often given at around 15 days, but degradation of PLGA is highly dependent on many factors, such as the chemical composition, additives such as acidic or basic species, a crystalline or amorphous morphology, size, shape, glass transition temperature and more [26].

In this study only the solid nanoparticles were made with the fluorescent-PLGA conjugates. But nanocapsules could also be made with these polymers. By this, potential leakage of dye will be avoided, and it can be investigated if the difference in biodistribution is caused by leakage of dye, or accumulation of the nanocolloids themselves. The main advantage of nanocapsules with an oily core is that several dye molecules can be incorporated. Less dye would be incorporated if the fluorescence is in the shell of the nanocapsules and not encapsulated. Here one percent of PLGA-DY-700 was used, more than this could be incorporated to yield stronger signals. To use PLGA-DY-700 to monitor the development of fluorescence from DiD loaded nanocapsules would be of value to compare the distributions seen.

The nanocapsules produced here show significant amounts of fluorescence from the bone marrow collected from the femur (Figure 4.15), also visible on the *in vivo* recordings (Figures 4.7-11). Animals injected with nanocolloids that had the dye covalently bound showed no accumulation of fluorescence in the bone marrow (Figures 4.13-14) and no fluorescence were detected in the collected bone marrow (Figure 4.17). More accumulation was seen into bones such as the spinal column and sternum in addition to the femurs in the mouse injected with free dye (Figure 4.9) than for the animals injected with nanocapsules. The highest amounts of fluorescence from the bone marrow was seen in the animals injected with PEGylated nanocapsules, both when DiD and DiI was used (Figure 4.17). This suggests that the PEGylated nanocapsules are more leaky than the unPEGylated nanocapsules. The addition of PEG chains might disturb the interactions between the dye and the PLGA, resulting in a release of dye through the polymer shell, or more seemingly that unPEGylated PLGA can pack itself tighter around the oily core, and that the addition of PEG chains leads to a less packed shell of polymer around the core. It has been shown that PEGylated carriers have a lower drug loading capacity, due to the steric interference of the PEG chains [11]. A higher amount of free dye might be present in the nanocapsule solution of the PEGylated nanocapsules, because of this.

Characterisations showed that the nanocapsules seemed to be affected by changes in the medium, such as addition of glucose and BSA (Figure 4.6), to a higher degree than the solid nanocolloids. They showed instability when monitored over a month (Figure 4.5). It seems that leakage of fluorescence from the nanocapsules, and then especially the PEGylated nanocapsules were experienced. The fluorescence lifetime investigations (Figure 4.12) also showed indication of rising levels the longer lifetime (Table 4.3) through the shift from the lifetime with the shorter lifetime towards a less uniform distribution of longer lifetimes. It is uncertain if the shift in lifetime suggest release of dye and that the short lifetime accumulating in the intestine (Figure 4.11) or if what is seen is the nanocapsules entering the enterohepatic circulations, something that have been indicated for these nanocolloids [31, 32]. The nanocapsules with an oily core seem to experience leakage, most distinct from the PEGylated nanocapsules. This could be because no stabiliser was used, and the formulation might improve from the use of a stabiliser such as a poloxamer. In some studies the nanocapsules have been produced without stabiliser [19, 20], others have utilised poloxamer 188 [30, 32]. The instability seen for the nanocapsules here might mean that the “trapped species” theory

for stabilisation does not hold up, at least not for lipid-polymer mixes, and only applicable for nanoemulsions [20].

An important consideration to make here is that if the carbocyanine dyes (Figure 1.5) leak from the nanocapsules, it is likely that drugs with related structures will also be released in a similar manner. An example of a lead compound where this could become an issue is tetradecylthioacetic acid, TTA, an synthetic modified fatty acid, shown to activate the peroxisome proliferator activated receptor (PPAR) [46, 47]. They regulate the expression of genes involved in lipid metabolism and are interesting as lipid lowering drugs [48]. TTA has been shown to attenuate dyslipidemia in male patients with type 2 diabetes mellitus and affect bone proliferation [46]. Nanocapsules would seem like a promising drug delivery vehicle for TTA, but the issues concerning leakage of the species incorporated need to be investigated.

5.4 Concluding remarks

We have successfully investigated the biodistribution of solid nanoparticles and nanocapsules with an oily core. The effect of PEGylation on the nanocolloids found was as expected. The PEGylated nanocapsules show indications of longer circulation times and seem to be captured by macrophages to a lesser degree than the unPEGylated nanocapsules. This is shown by higher uptake into the liver and higher levels present in the intestine, indicated as the route of excretion of these nanocolloids is through the lymphatic system, and have also been showed by others [31, 32].

This study suggest that there is leakage of dye from the nanocapsules, clearly indicated by the visible accumulations seen from the nanocapsules (Figure 4.7-11), and no such accumulation was visible for the solid nanoparticles (Figure 4.12-13). Measurements of fluorescence in the bone marrow (Figure 4.15), also showed strong fluorescence in the samples collected from mice injected with nanocapsules, and no such fluorescence was found in the samples collected from mice injected with the solid nanoparticles. When taken together with the characterisations that showed larger instability of the nanocapsules than the solid nanoparticles (Figure 4.6) it appears that leakage of fluorophore form the oily core had occurred.

Nanocolloids made from polymers that have the fluorescent dye conjugated to the polymer seem to have an advantage and would give more reliable results with more ease of analysis, as the nanocapsules produced here showed leakiness of the incorporated dye. An important

consideration to be made here is that drugs with similar structures to that of the carbocyanine dyes also might be leaked from the nanocolloid. One will also have to further evaluate the safety of the dyes *in vivo.*

5.5 Future studies

The nanocapsules with an oily core were produced without stabiliser. They were shown to be leaky. It would therefore be interesting to compare the nanocapsules made with and without stabiliser. This could give indications of differences in stability, and if the "trapped species" theory holds up [19]. Further investigations around the leakiness of these nanocapsules would have to be preformed. It is now seen that it is important that any residual free dye in the nanocolloids are dialysed or otherwise removed before evaluation.

Since the degradation of PLGA nanocolloids are dependent of several factors, and difficult to predict, the biodistributions of all the nanocolloids should be traced for longer than 24 hours to enable further interpretation of the sustainable release abilities, accumulation and further degradation and elimination *in vivo.*

It would be particularly interesting to determine if the differences in biodistributions between nanocapsules and nanoparticles are due to leakage of fluorophore or due to real differences in biodistributions between the two colloids. I would like to follow and compare the development of fluorescence from DiD loaded nanocapsules with the solid nanoparticles and to further compare this with development from free dye. Also the production of nanocapsules with covalently linked fluorophores could give answers around how well the carbocyanine dyes are retained in the nanocapsules. It is possible to incorporate the DY-700 in the polymeric shell, and a green-fluorescent carbocyanine dye into the oily core. Although green fluorescence is not as suited as NIR fluorescent dyes, it would be possible to get an idea of differences in biodistribution between the two different fluorophores. Small animal imager for green fluorescence is present at the molecular imaging centre (MIC) at UiB.

It would be useful to collect tissue samples at several time points for *ex vivo* investigations, preferably for all the nanocolloids used. This was done at 3 hours for the solid nanoparticles conjugated to rhodamine, but due to problems with the method at this point, the colloid administered showed only traces of fluorescence. Nanocolloids covalently linked to Texas red are promising drug discovery tools, as the images from in vivo examinations could be directly compared to counts made *ex vivo* and in principle, immune-staining can be preformed to

detect which cell types that accumulate the nanoparticles. Further examinations of solid nanoparticles would because of this preferably be conducted with PLGA-DY-700.

When the parameters above have been investigated, it would be very interesting to use these nanocarriers as theranostics to investigate a metastatic tumour model in rodents. The cancer cells could be labelled with green florescence, e.g. green fluorescent protein, while the nanocolloids is coupled whit a red fluorophore, such as DY-700. In addition one or more chemotherapeutics would be incorporated into the nanocolloid together with a targeting moiety, such as folate. One could then investigate both the ability of the nanocolloids to locate and accumulate in the tumour cells, and also the effectiveness of the chemotherapeutics in the same model.

When the parameters above have been investigated, these nanocarriers could become useful as theranostics for instance to investigate a metastatic tumour model in rodents. One can imagine a system where the cancer cells express green fluorescent protein, while the nanocolloids are labelled with a red fluorophore, such as DY-700. In addition one or more chemotherapeutics can be incorporated into the nanocolloid together with a tumour-targeting moiety, for instance folate. The location of the metastases can then be detected by in vivo imaging, and also if the nanocolloids accumulate in tumour-infiltrated tissues or organs. Moreover, one can detect the efficacy of the nanocolloids by measuring if the fluorescent signal from the tumours decreases. Then, we can clearly state that the nanocolloids are multi-modal.

References:

1. Adair, J.H., et al., *Nanoparticulate Alternatives for Drug Delivery.* ACS Nano, 2010. **4**(9): p. 4967-4970.
2. Sahoo, S.K., et al., *Residual polyvinyl alcohol associated with poly (d,l-lactide-co-glycolide) nanoparticles affects their physical properties and cellular uptake.* Journal of Controlled Release, 2002. **82**(1): p. 105-114.
3. Letchford, K. and H. Burt, *A review of the formation and classification of amphiphilic block copolymer nanoparticulate structures: micelles, nanospheres, nanocapsules and polymersomes.* European Journal of Pharmaceutics and Biopharmaceutics, 2007. **65**(3): p. 259-269.
4. Hans, M.L. and A.M. Lowman, *Biodegradable nanoparticles for drug delivery and targeting.* Current Opinion in Solid State and Materials Science, 2002. **6**(4): p. 319-327.
5. Nehilla, B.J.A., P.G.; Desai, T. A., *Surfactant-Free, Drug-Quantum-Dot Coloaded Poly(lactide-co-glycolide) Nanoparticles: Towards Multifunctional Nanoparticles.* ACS Nano, 2008. **2**(3): p. 538-544.
6. Altınoğlu, E.İ. and J.H. Adair, *Near infrared imaging with nanoparticles.* Wiley Interdisciplinary Reviews: Nanomedicine and Nanobiotechnology, 2010. **2**(5): p. 461-477.
7. Herfindal, L.N., I. M.; Milankovic, S.M., *Bruk av nanokolloidar i behandling av sjukdomer.* Naturen, 2012. **In Press**.
8. Ravi Kumar, M.N.V., U. Bakowsky, and C.M. Lehr, *Preparation and characterization of cationic PLGA nanospheres as DNA carriers.* Biomaterials, 2004. **25**(10): p. 1771-1777.
9. Felleskatalogen. 2012 30.05.12]; Available from: http://www.felleskatalogen.no/medisin/abraxane-celgene-572142#egenskap.
10. *Statens Legemiddelverk SPC Abraxane*. p. http://www.legemiddelverket.no/custom/Preparatsok/prepSearch____80333.aspx?SearchID=71e5a0e4-33f4-41ce-8b1e-615e3c11d075.
11. Makadia, H.K. and S.J. Siegel, *Poly Lactic-co-Glycolic Acid (PLGA) as Biodegradable Controlled Drug Delivery Carrier.* Polymers, 2011. **3**(3): p. 1377-1397.
12. Maeda, H., *The enhanced permeability and retention (EPR) effect in tumor vasculature: the key role of tumor-selective macromolecular drug targeting.* Advances in Enzyme Regulation, 2001. **41**(1): p. 189-207.
13. Lim, Y.T., Noh, Y.-W., Han, J. H., Cai, Q.-Y., Yoon, K.-H. and Chung, B. H. , *Biocompatible Polymer-Nanoparticle-Based Bimodal Imaging Contrast Agents for the Labeling and Tracking of Dendritic Cells.* Small, 2008(4): p. 1640–1645.
14. Dufort, S., et al., *Optical small animal imaging in the drug discovery process.* Biochimica et Biophysica Acta (BBA) - Biomembranes, 2010. **1798**(12): p. 2266-2273.
15. Sun, Y., et al., *Superparamagnetic PLGA-iron oxide microcapsules for dual-modality US/MR imaging and high intensity focused US breast cancer ablation.* Biomaterials, (0).
16. Kumar, R., et al., *In Vivo Biodistribution and Clearance Studies Using Multimodal Organically Modified Silica Nanoparticles.* ACS Nano, 2010. **4**(2): p. 699-708.
17. Mahapatro, A. and D.K. Singh, *Biodegradable nanoparticles are excellent vehicle for site directed in-vivo delivery of drugs and vaccines.* J Nanobiotechnology, 2011. **9**: p. 55.
18. Aulton, M., *Aulton`s Pharmaceutics - The design and manufacture of medicines*, ed. A.M. E.2007: Churchill Livingstone Elsevier.
19. Delmas, T., et al., *How To Prepare and Stabilize Very Small Nanoemulsions.* Langmuir, 2011. **27**(5): p. 1683-1692.
20. Gravier, J.N., F. P.; Delmas T.; Mittler F.; Couffin A. C.; Vinet F.; Texier, I. , *Lipidots: competetive organic alternative to quantom dots for in vivo fluorescence imaging.* Journal of Biomedical Optics, 2011. **16**(9).

21. Instruments, M. *Zeta potential An introduction in 30 minutes. Technical note.* 15.04.2012].
22. Fessi, H., et al., *Nanocapsule formation by interfacial polymer deposition following solvent displacement.* International Journal of Pharmaceutics, 1989. **55**(1): p. R1-R4.
23. Govender, T., et al., *PLGA nanoparticles prepared by nanoprecipitation: drug loading and release studies of a water soluble drug.* Journal of Controlled Release, 1999. **57**(2): p. 171-185.
24. Chacón, M., et al., *Optimized preparation of poly d,l (lactic-glycolic) microspheres and nanoparticles for oral administration.* International Journal of Pharmaceutics, 1996. **141**(1–2): p. 81-91.
25. Delmas, T.C., A. C.; Bayle, P. A.; de Crecy, F.; Neumann E.; Vinet, F.; Bardet, J.; Texier, I., *Preparation and characterization of highly stable lipid nanoparticles with amorphous core of tunable viscosity.* Journal of Colloidal and Interface Science, 2011(360): p. 471-481.
26. Anderson, J.M. and M.S. Shive, *Biodegradation and biocompatibility of PLA and PLGA microspheres.* Advanced Drug Delivery Reviews, 1997. **28**(1): p. 5-24.
27. Zheng, C., et al., *Indocyanine green-loaded biodegradable tumor targeting nanoprobes for in vitro and in vivo imaging.* Biomaterials, 2012. **33**(22): p. 5603-5609.
28. Jubeli, E.M., L; Nicolas, V.; Barratt, G., *Preparation of E-selectin-targeting nanoparticles and preliminary in vitro evaluation.* International Journal of Pharmaceutics, 2012. **426**: p. 291-301.
29. Clifton, G.T., et al., *Folate receptor α: A storied past and promising future in immunotherapy.* Human Vaccines, 2011. **7**(2): p. 183-190.
30. Mosqueira, V.C.F.L., P.M.; Bories, C.; Legrand, P.; Devissaguet, J. P; Barratt, G. , *Efficacy and pharmacokinetics of intravenous nanocapsule formulations of Halofantrine in plasmoudium berghei-infected mice.* Anitmicrobial agents and Chemoterapy, 2004. **48**(4): p. 1222-1228.
31. Das S.; Chaudhury, A., *Recent Advances in Lipid Nanoparticle Formulations with Solid Matrix for Oral Drug Delivery.* PharmSciTech. , 2011. **12**(1): p. 62-76.
32. Tosi, G., et al., *NIR-labeled nanoparticles engineered for brain targeting: in vivo optical imaging application and fluorescent microscopy evidences.* Journal of Neural Transmission, 2011. **118**(1): p. 145-153.
33. A., S., *Alternatives to the use of animals*, in *UiB Animal research course*2012.
34. John V, F., *In vivo near-infrared fluorescence imaging.* Current Opinion in Chemical Biology, 2003. **7**(5): p. 626-634.
35. Jin, Z. and N. Hildebrandt, *Semiconductor quantum dots for in vitro diagnostics and cellular imaging.* Trends in Biotechnology, (0).
36. Reul, R., et al., *Near infrared labeling of PLGA for in vivo imaging of nanoparticles.* Polymer Chemistry, 2012. **3**(3): p. 694-702.
37. Goutayer, M., et al., *Tumor targeting of functionalized lipid nanoparticles: Assessment by in vivo fluorescence imaging.* European Journal of Pharmaceutics and Biopharmaceutics, 2010. **75**(2): p. 137-147.
38. Invitrogen. 2012. Available from: http://www.invitrogen.com/site/us/en/home/support/Product-Technical-Resources/Product-Spectra.307lip.html.
39. [cited 2012 22.04.2012]; Available from: http://www.vectorlabs.com/catalog.aspx?prodID=427.
40. Gref, R., et al., *Biodegradable Long-Circulating Polymeric Nanospheres.* Science, 1994. **263**(5153): p. 1600-1603.
41. Sand, O.S., Ø. V.; Haug E., *Menneskets fysiologi*, 2001, Gyldendal Akademisk. p. 309.
42. Mosqueira, V.C.F., et al., *Relationship between complement activation, cellular uptake and surface physicochemical aspects of novel PEG-modified nanocapsules.* Biomaterials, 2001. **22**(22): p. 2967-2979.

43. Müller, R.H., D. Rühl, and S.A. Runge, *Biodegradation of solid lipid nanoparticles as a function of lipase incubation time.* International Journal of Pharmaceutics, 1996. **144**(1): p. 115-121.
44. CANNON, B. and J. NEDERGAARD, *Brown Adipose Tissue: Function and Physiological Significance.* Physiological Reviews, 2004. **84**(1): p. 277-359.
45. Avgoustakis, K., et al., *Effect of copolymer composition on the physicochemical characteristics, in vitro stability, and biodistribution of PLGA–mPEG nanoparticles.* International Journal of Pharmaceutics, 2003. **259**(1–2): p. 115-127.
46. Stunes, A.K., et al., *Skeletal effects of the saturated 3-thia Fatty Acid tetradecylthioacetic Acid in rats.* PPAR Res, 2011. **2011**: p. 436358.
47. Vigerust, N.F., et al., *Fish oil and 3-thia fatty acid have additive effects on lipid metabolism but antagonistic effects on oxidative damage when fed to rats for 50 weeks.* The Journal of Nutritional Biochemistry, (0).
48. Walker, R.W.C., *Clinical Pharmacy and Therapeutics*2007, Churchill Livingstone Elsevier.